TRABAJOS DE FIN DE GRADO / FIN DE MÁSTER

Escuela de Ingeniería y Arquitectura Universidad Zaragoza

DECLARACIÓN DE AUTORÍA Y ORIGINALIDAD

(Este documento debe acompañar al Trabajo Fin de Grado (TFG)/Trabajo Fin de Máster (TFM) cuando sea depositado para su evaluación).

D./Dª. Álvaro García Aranda,

con nº de DNI 25360946L en aplicación de lo dispuesto en el art. 14 (Derechos de autor) del Acuerdo de 11 de septiembre de 2014, del Consejo de Gobierno, por el que se aprueba el Reglamento de los TFG y TFM de la Universidad de Zaragoza,

Declaro que el presente Trabajo de Fin de (Grado/Máster) Grado en Ingeniería Mecánica, (Título del Trabajo) Simulation of induction heating of a cylindrical steel rod

es de mi autoría y es original, no habiéndose utilizado fuente sin ser citada debidamente.

Zaragoza, 23 de octubre de 2018

Fdo: Álvaro García Aranda

Simulation of induction heating of a cylindrical steel rod

by
Álvaro García Aranda

Bachelor-Thesis

Faculty of Mechanical Engineering
RWTH Aachen University – Universidad de Zaragoza

This thesis was supervised by:
Research assistant: M.Sc. A. Rajaei
Responsible professor: Univ.-Prof. Dr.-Ing C. Broeckmann
Institute for Materials Applications in Mechanical Engineering (IWM), RWTH Aachen

Aachen, August 2018

Table of Contents

Nomenclature

SYMBOL	DESCRIPTION
t	Time
Φ_B	Magnetic flux
$\mathcal{E}$	Electromotive force (EMF)
B	Magnetic field vector
H	Magnetic field intensity vector
J	Electric current density vector
f	Frequency
μ	Magnetic permeability
μ_0	Magnetic permeability in vacuum
μ_r	Relative magnetic permeability
ρ	Electric resistivity
ω	Angular velocity
δ	Skin depth
J_r	Electric current density at a radius r
J_R	Electric current density at the cylinder radius R
H_r	Magnetic field intensity at a radius r
H_R	Magnetic field intensity at the cylinder radius R
P_w	Power loss per unit volume
$\wp_w$	Power loss per square unit
$\wp_x$	Power loss at a height x
R	Electric resistance
I	Electric current
V	Voltage or volume
E	Electric energy
P_{Joule}	Joule power
$\dot{Q}$	Heat
$\dot{q}$	Specific heat flux
λ	Thermal conductivity
α	Convection coefficient
U	Internal energy of a system
c	Specific heat
c_p	Specific heat (constant pressure)
$\dot{Q}_{source}$	Heat generated by an energy source

∇T	Temperature gradient
$\Theta \text{ or } T$	Temperature
Θ_s	Temperature in the surface of the cylinder
Θ_c	Temperature in the center of the cylinder
τ	Normalized time
Θ_m	Mean temperature in the cylinder
σ	Electrical conductivity
T_0	Initial temperature in the rod
T_{air}	Temperature of the surrounding air
t_{max}	Total time of all sequential simulations
$T_{peak,i}$	Peak temperature in simulation i
v	Velocity of the coil (constant)
$z_{coil}(t)$	Position of the coil with time
$v_{coil}(t)$	Velocity of the coil with time

1 Introduction

Induction hardening is a thermal treatment process, which uses the heat generated by electric currents that are induced in a work-piece by electromagnetic induction, to heat this work-piece to cooling it rapidly after that, so that we can obtain a hardened work-piece. [1]. It is based on the phenomenon of electromagnetic induction discovered initially by Michael Faraday and extended by Maxwell and Lenz.

Electromagnetic induction is a phenomenon that occurs in conductive materials when exposed to a variable magnetic flux [2]. This exposure produces an electromotive force that is induced in the conductive material, which generates electric currents in the material, called eddy currents. Eddy current or Foucault currents are electric currents generated in a conductive material a result of being exposed to a variable magnetic flux, as stated in Faraday's law [2].

Induction heating is used in dilatometric test as the heat source. During the heating, the length change is measured in order to monitor phase transformations or to perform compression tests. In these tests, the heat is dissipated towards the sample supports at the sample's ends. This creates temperature gradients that grow with time and that influence the length change. Therefore, these temperature gradients have to be considered in the analysis of the of the transformation kinetics and compression tests.

Induction hardening is used for surface hardening of work-pieces with a complex geometry, like gears. To study the application of this method, a simulation in FEM program coupling an electromagnetical analysis and a heat transfer analysis can be used.

2 Physical & technical fundaments of induction hardening

Induction heating is based on three main principals [1]:

- Electromagnetic induction
- Skin effect and eddy currents
- Joule heating and heat transfer

This three concepts will be explained in the following sections, as well as the hardening process by induction in steels.

2.1 Electromagnetic induction

As explained, electromagnetic induction is the generation of an electromotive force in a conductive material when this one is exposed to a variable magnetic field. The cause of the generation of the electromotive force is the variation of the magnetic flux through the material [2].

The magnetic flux is defined as the number of magnetic field lines that pass through the work-piece. Supposing a work-piece with a transversal area $\boldsymbol{S}$, through which the lines of a magnetic field $\boldsymbol{B}$ pass, the magnetic flux is:

$$\Phi_B = \mathbf{B} * \mathbf{S} = \mathrm{B} * \mathrm{S} * \cos(\Theta) \qquad (2.1.01)$$

Θ is the angle between the magnetic field vector **B** and the perpendicular direction to the surface S. This is illustrated in Figure 1.

As the electromotive force is generated by the variation of the magnetic flux, to generate this EMF, any of the three components of Eq. (2.1.01) or a combination of them can be changed. One of the most used is the change in the angle. This is the base of the functioning of the alternators, which are used to generate electric current with a circular motion of a turbine. But in the case treated here, the one changed was the magnetic field by using an alternate current.

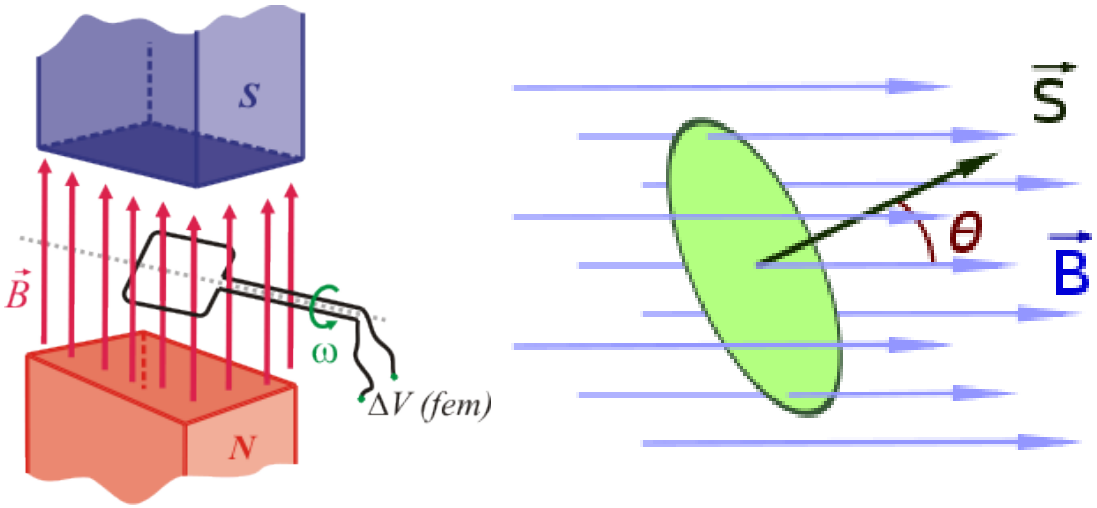

Figure 1: Illustration of electromagnetic induction (left) and of the components of the magnetic flux.

Faraday's law

Faraday's law of induction is the base for one of the four laws of Maxwell, which describe the behavior of electromagnetism for macroscopical systems.

This law explains how a magnetic field will interact with an electric circuit to produce the electromotive force [2]. The most widespread statement of the law is:

"The induced electromotive force in any closed circuit is equal to the negative of the time rate of change of the magnetic flux enclosed by the circuit".

As this law is just the base for the complete law of induction, it is only usable for a closed circuit with an infinitely thin wire.

As explained in the previous section, the generation of the electromotive force is due to a variation in the magnetic flux Φ_B through an hypothetical surface $\Sigma(t)$, which is the surface bounded by the wire of the closed circuit and can be variable throughout time. Then, the magnetic flux is defined as the surface integral of the magnetic field $\boldsymbol{B}$:

$$\Phi_B = \iint_{\Sigma(t)} \boldsymbol{B}(\boldsymbol{r}, t) * d\boldsymbol{A} \qquad (2.1.02)$$

$\boldsymbol{A}$ is the surface through which the magnetic field passes. Knowing how the flux changes, the generated electromotive force can be obtained, since it is proportional to the rate of variation of the magnetic flux with time:

$$\mathcal{E} = -\frac{d\Phi_B}{dt} \qquad (2.1.03)$$

The direction of the electromotive force is given by the Lenz's law.

Maxwell-Faraday equation

Maxwell-Faraday's law of electromagnetic induction is the generalization of the previous law to be applicable to any system. It explains that a time-changing

magnetic field $\boldsymbol{B}$ will always be accompanied by a space-changing electric field $\boldsymbol{E}$, and vice versa. This equation is the following [6]:

$$\nabla \mathrm{x}\, \mathbf{E} = -\frac{\partial \boldsymbol{B}}{\partial t} \qquad (2.1.04)$$

Lenz's law

The direction of the electromotive force can be obtained from Lenz's law. This law states that the induced current will flow in the direction to cause a magnetic field that opposes to the one that produced it. This is the reason to the negative sign in Eq. (2.1.03).

Eddy currents

Eddy currents are the electric currents generated by electromagnetic induction in any conductive material. They flow in closed loops perpendicular to the lines of the magnetic field [2].

The magnitude of these currents is proportional to the strength of the magnetic field, the area of loop, and the rate at which the flux changes with time. They also depend on the electric resistivity of the material, being higher the lower the resistivity is.

The flow direction of the eddy currents is given by the Lenz's law, so that their flow direction will be the one that opposes to the change of magnetic flux.

Eddy currents are considered in many applications, like in alternators, as a cause of energy loss. They require special constructions, like using laminated cores, to minimize them. On the other hand, eddy currents can be used as a source of heat in heating processes, like the one we are treating here, or to detect cracks and flaws in metal parts.

Figure 2 shows a metal sheet, where eddy currents are being induced by a magnet close to it. The sheet is moving past the magnet, so that the magnetic flux changes, generating the eddy currents. At the left part of the sheet, the magnetic field is becoming higher. The eddy currents will flow in the direction that oppose the increase of the magnetic field, generating a magnetic field in the opposite direction, that is, eddy currents will flow in a counterclockwise direction. In the right side happens the opposite, as the magnetic field is decreasing. Therefore, the magnetic field generated by the eddy currents will have the same direction as the main magnetic field. In this case, eddy currents flow in a clockwise direction.

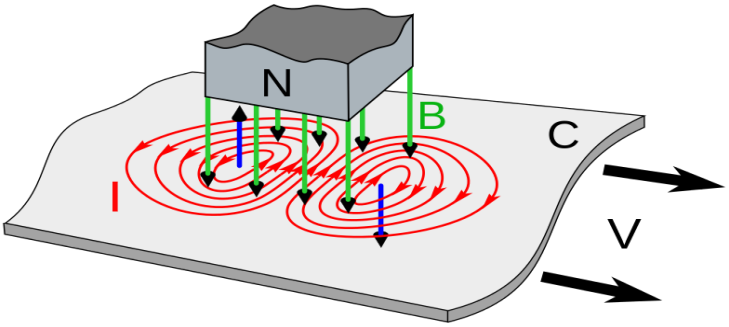

Figure 2: Eddy currents in a moving metal sheet

Electromagnetic induction of a cylinder

In this section, the most important parameters in electromagnetic induction that will be in the results of the electromagnetic part of the Co-Simulation are described. Most of this definitions come from [3].

Magnetic field and current density

Many practical work pieces are cylindrical in form, as the one treated in the simulation, are heated by being placed in a solenoid or using single coils. The axial magnetic field, which changes with time following a sinus function, causes eddy currents to flow in circular paths in the work-piece. The following equations are described for cylindrical coordinates. The base of this equations can be derived from the induction of a semi-infinite slab, which is the simplest geometry to understand electromagnetic induction in a work-piece.

To obtain the magnetic field $\boldsymbol{H}$, as well the current density $\boldsymbol{J}$, the diffusion equations are used:

$$\nabla^2 \boldsymbol{H} = \frac{\mu}{\rho}\frac{\partial \boldsymbol{H}}{\partial t} \quad ; \quad \nabla^2 \boldsymbol{J} = \frac{\mu}{\rho}\frac{\partial \boldsymbol{J}}{\partial t} \tag{2.1.05}$$

μ is the magnetic permeability and ρ the electric resistivity of the material. Taking the one for the magnetic field:

$$\frac{d^2\boldsymbol{H}}{dr^2} + \frac{1}{r}\frac{d\boldsymbol{H}}{dr} - k^2\boldsymbol{H} = 0, \quad \text{where} \quad k^2 = \frac{j\omega\mu}{\rho} = 2j\alpha^2 \tag{2.1.06}$$

This is one of the Bessel's equations, as the geometry is cylindrical. Therefore, the solution will be in Bessel functions of the form:

$$H = AI_0(kr) + BK_0(kr) \tag{2.1.07}$$

where I_0 and K_0 are Bessel functions of order zero [4]. The solution to this equation is in terms of ber and bei and similar functions. These are cylindrical equivalents of the solution of the semi-infinite slab.

$$\frac{H_r}{H_R} = \frac{ber\sqrt{2}\alpha r + jbei\sqrt{2}\alpha r}{ber\sqrt{2}\alpha R + jbei\sqrt{2}\alpha R} \tag{2.1.08}$$

where R is the radius of the cylinder and r is any radius, smaller than R;

(2.1.09)

$$J_r = \sqrt{2\alpha H_R}\frac{ber'\sqrt{2}\alpha r + jbei'\sqrt{2}\alpha r}{ber\sqrt{2}\alpha R + jbei\sqrt{2}\alpha R}$$

$$\frac{J_r}{J_R} = \frac{ber'\sqrt{2}\alpha r + jbei'\sqrt{2}\alpha r}{ber'\sqrt{2}\alpha R + jbei'\sqrt{2}\alpha R} \quad (2.1.10)$$

$$\left|\frac{J_r}{J_R}\right| = \frac{\sqrt{ber'^2\sqrt{2}\alpha r + bei'^2\sqrt{2}\alpha r}}{\sqrt{ber'^2\sqrt{2}\alpha R + bei'^2\sqrt{2}\alpha R}} \quad (2.1.11)$$

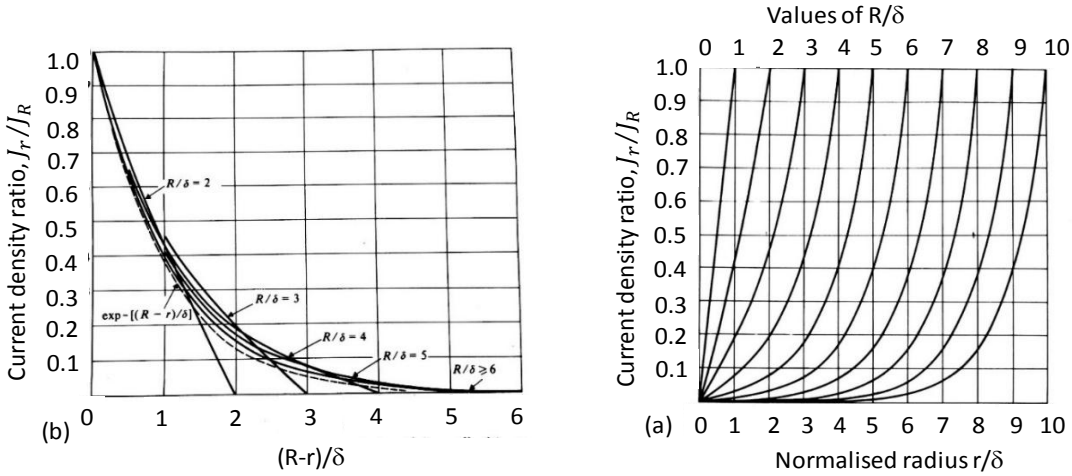

Figure 3: Current density distribution in a solid cylinder (left) & generalized form of the previous graphic (right) [3]

Figure 3 shows this current density ratio for different values of r/δ and of R/δ.

Power loss

The loss of power is the amount of energy per unit of time that is lost in the form of heat by Joule effect. It is defined :

$$P_w = \frac{1}{2}\int_0^R \rho\,|J_{rm}|^2 2\pi r dr$$

J_{rm} is the maximal value of the current density in a radius r. Using the previous equations:

$$P_w = \sqrt{2}\pi\rho\alpha {H_{Rm}}^2 R\left[\frac{ber'(\sqrt{2}\alpha R)ber\sqrt{2}\alpha R + bei'(\sqrt{2}\alpha R)bei\sqrt{2}\alpha R}{ber^2\sqrt{2}\alpha R + bei^2\sqrt{2}\alpha R}\right] \quad (2.1.12)$$

To simplify this expression, the variable p is defined:

$$p = \frac{\sqrt{2}}{\alpha R}\frac{bei'(\sqrt{2}\alpha R)bei\sqrt{2}\alpha R + ber'(\sqrt{2}\alpha R)ber\sqrt{2}\alpha R}{ber^2\sqrt{2}\alpha R + bei^2\sqrt{2}\alpha R}$$

Now, writting Eq. (2.3.12) in terms of p:

$$P_w = \mu\pi f {H_{Rm}}^2 (l_w A_w)p \quad (2.1.13)$$

l_w is the length and A_w the transversal area of the cylinder.

The power loss per unit square can also be defined (also called power density)

$$\wp_w = \mu\pi f {H_{Rm}}^2 \frac{R}{2} p \tag{2.1.14}$$

From this result, it can be inferred that the power loss is proportional to ${H_{Rm}}^2$. Knowing this, it can be also deduced that the power loss is also proportional to the square of the electric current density, as $\boldsymbol{J = \nabla x H}$**.** This dependence will be shown in the simulation.

Effect of the proximity of the coil

The proximity of the coil is the distance between the inner radius of the coil and the radius of the rod. One process where the proximity is important is scanning hardening, which is the one treated in the simulation. In this process, the surface a cylindrical rod is heated using only a single coil near the surface that moves along the rod. This process is implemented using heavy currents flowing in the coil. Because the coil, compared to the cylinder radius R, is near the surface, it is usually valid to treat this as a line current at a distance x from flat plane.

The current density J at a point distant x from the center line due to a current intensity I at height h above the plane is given by:

$$J = \frac{I}{h\pi} \frac{1}{1 + (x/h)^2} \tag{2.1.15}$$

From Eq. (2.3.14) the ratio of power density at x to the maximum power density can be obtained:

$$\frac{\wp_x}{\wp_{max}} = \left[\frac{1}{1 + \left(\frac{x}{h}\right)^2} \right]^2 \tag{2.1.16}$$

with:

$$\wp_{max} = \frac{\rho}{\delta} \frac{I^2}{\pi^2 h^2} \tag{2.1.17}$$

This is a simplified approach, but it illustrates the effect of the proximity parameters:

- The maximum loss, directly under the conductor, falls off as the square of the height h. This shows the importance proximity between coil and rod.
- The power density falls away rapidly with distance from the maximum loss point.

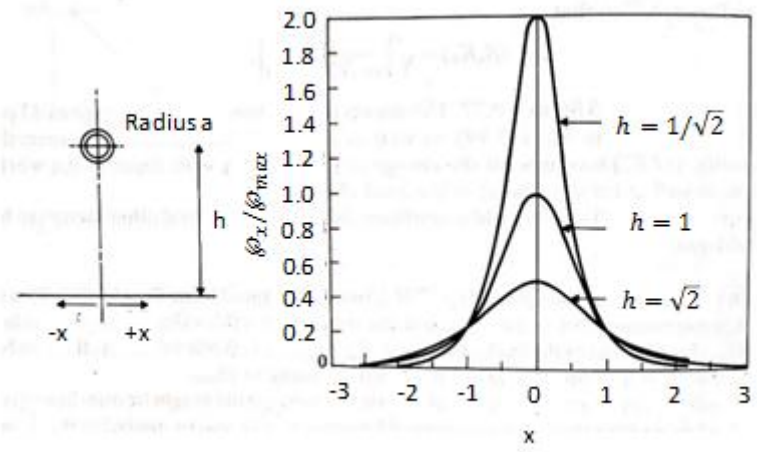

Figure 4: Proximity effect and $\wp_x/\wp_{max}$ distribution (left) & variation of temperature in a cylinder with the radius r in a normalized time τ [3]

Joule heating

Joule heating or Joule effect is a phenomenon that occurs in materials with an electrical resistivity different from zero when conducting electricity [2]. A fraction of the kinetic energy of the electrons turns into heat due to the collisions with other electrons. This heat causes the increase of the temperature of the material.

Joule effect is considered as undesirable in electric applications because it causes energy losses. This is one of the reasons why eddy currents are considered an undesirable effect. But, on the other hand, this effect can be used for heating processes, like the one treated here.

The most basic form of the Joule heating can be obtained from the Ohm law and the expression of the electric energy in an electric circuit:

$$V = I \cdot R$$

$$E = V \cdot I \cdot t$$

V is the voltage, I the electric current, E the electric energy, t the time and R the electric resistance, which is proportional to the electric resistivity.

By putting together these two equations:

$$E = I^2 \cdot R \cdot t$$

Knowing that the power is the energy per unit time, one obtains:

$$P_{Joule} = I^2 \cdot R \tag{2.1.18}$$

Hence, it can be inferred that the Joule power P_{Joule} will be higher the higher the resistivity is. This is why, for example, the temperature in a copper does not increase very much compared to the temperature in steel, which has a higher resistivity.

A more general expression for the Joule power in any system can be defined:

$$\iiint_V \boldsymbol{J} \cdot \boldsymbol{E} \cdot dV \tag{2.1.19}$$

V in this case is the volume of the system, while $\boldsymbol{J}$ is the electric current density through the system and $\boldsymbol{E}$ the electric field in the system.

2.2 Skin effect

As shown in Figure 5, the electrical current of the surrounding coils generates a magnetic field, whose lines go through the rod, generating electrical currents in it. Due to the thickness of the rod, the electrical currents are much stronger in the surface area than in the center. This is the Skin effect [3], which happens especially at high frequencies of magnetic field. Current density falls off from the surface to the center. The following section will be explained using a semi-infinite slab to simplify the definition of the skin effect.

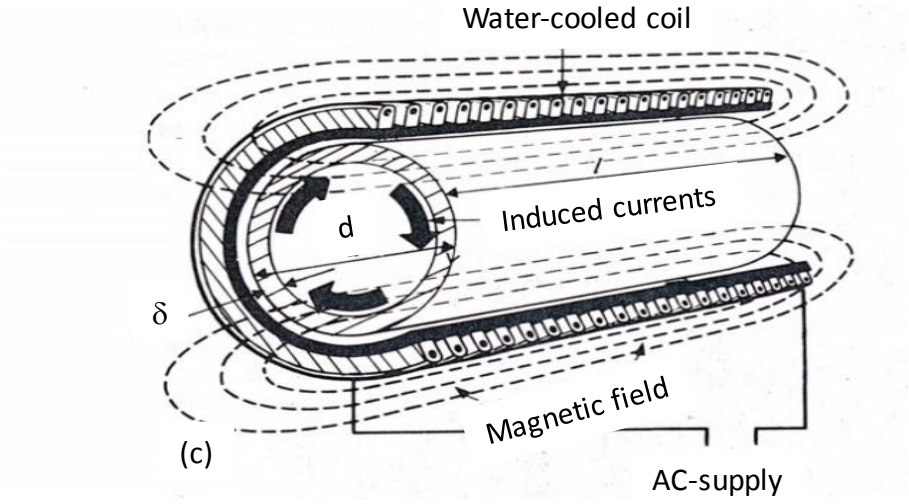

Figure 5:Example of induction heating in a cylindrical rod [3]

Skin effect for a semi-infinite slab

Figure 6 shows a slab close to a coil. The coil produces a magnetic field H_0 at the surface of the slab. Assuming that the coil is so near the slab surface, the magnetic field H_0 of the coil is approximately the same as the one on the surface of the slab. For induction heating, the applied magnetic field's magnitude changes with time. This time-changing H_0 will produce eddy currents in the z direction.

The boundary conditions are:

$$H_{x(y=0)} = H_{0m}\cos(\omega t)$$
$$\begin{cases} H_y \\ H_z \end{cases} = 0 \; everywhere \qquad (2.2.01)$$

H_{0m} is the peak value of the magnetic field H_x at the surface (y=0).

To obtain the distribution of the magnetic field, the diffusion equation for $\boldsymbol{H}$ is used:

$$\nabla^2 \boldsymbol{H} = \frac{\partial^2 \boldsymbol{H}}{\partial x^2} + \frac{\partial^2 \boldsymbol{H}}{\partial y^2} + \frac{\partial^2 \boldsymbol{H}}{\partial z^2} \qquad (2.2.02)$$

Knowing that, in the y-axis and in the z-axis there are no variations in the magnetic field, Eq. (2.2.02) can be reduced to:

$$\frac{\partial^2 H_x}{\partial y^2} = \frac{\mu}{\rho}\frac{\partial H_x}{\partial t}$$

A solution of this is of the form $H_x = H_x(y)\cos(\omega t)$, where $H_x(y)$ is the variation of H_x with depth y. Substituting $\alpha^2 = \frac{\mu}{2\rho}\omega$ and $k^2 = 2j\alpha^2$:

$$H_x = A_1 \exp(ky) + A_2 \exp(-ky)$$

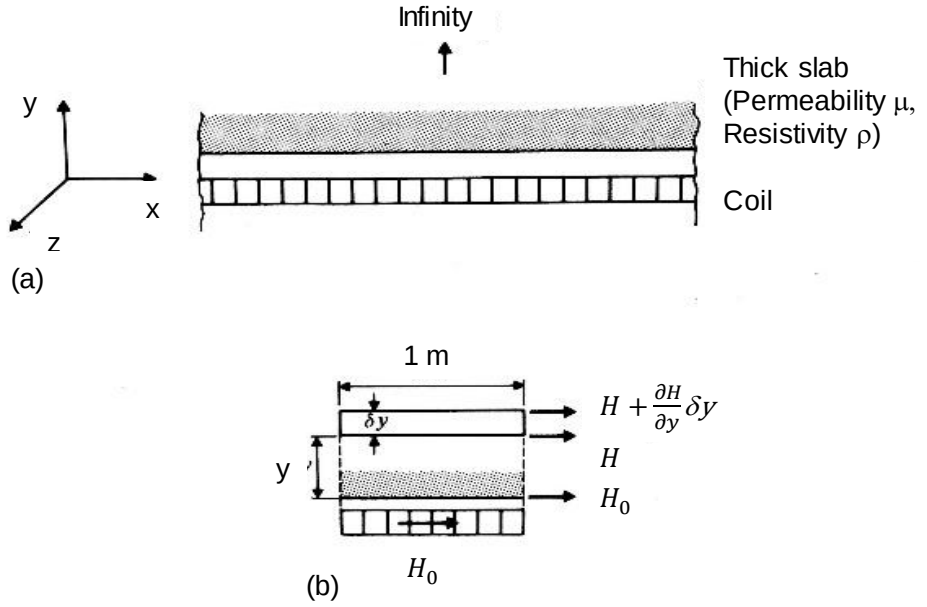

0

Figure 6: Illustration of skin effect on a semi-infinite slab [3]

To find A_1 and A_2, the boundary conditions are used. Operating with them:

$$H_x(y) = H_{0m} \exp(\alpha y)\, cos(\omega t - \alpha y) \qquad (2.2.03)$$

This is a very important solution in induction heating. With this, the magnetic field intensity at any position of y in the slab can be obtained.

Skin depth

From Eq. (2.3.01) is known that the magnetic field at the surface ($y = 0$) is $H_x = H_{0m}\cos(\omega t)$. The magnitude of the magnetic field at any other depth in the slab falls of exponentially with y. When $y = {}^{1}/_{\alpha}$, the magnitude falls to e^{-1} This depth is a very important parameter and is called *skin depth* or *depth of penetration* δ. The variation of H with the depth is shown in Figure 7. It is often useful to employ the ratio ${}^{y}/_{\delta}$ in induction heating work.

The skin depth is defined:

$$\delta = \sqrt{\frac{2\rho}{\mu\omega}} \qquad (2.2.04)$$

where $\mu = \mu_r \mu_0$ is the realtive magnetic permeability.

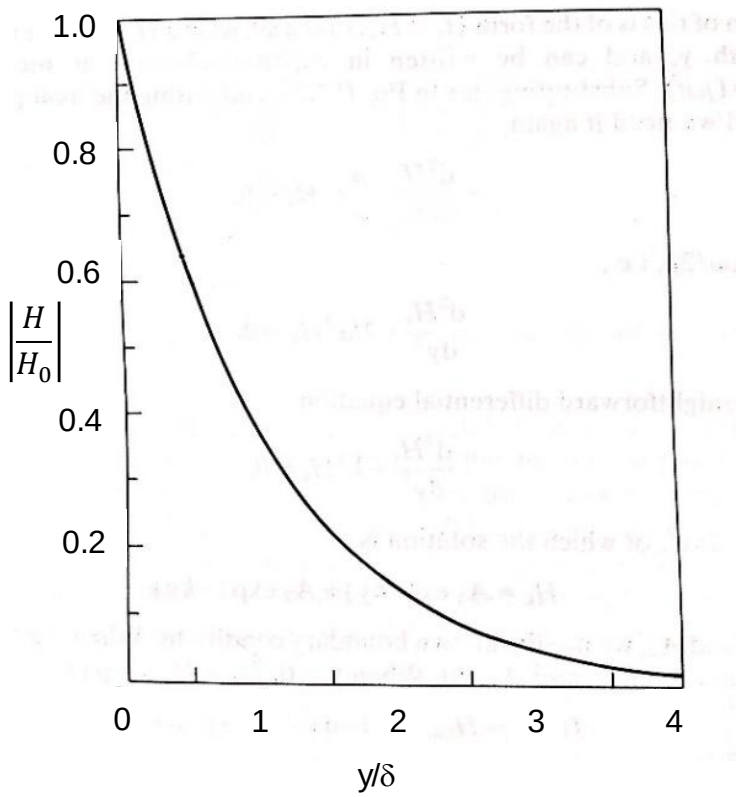

Figure 7: Variation of the magnetic field H with the depth [3]

2.3 Heat transfer

Heat transfer mechanisms

There are three heat transfer mechanisms [5]:

- Conduction
- Convection
- Radiation

For the problem treated in the thesis, it will not be taken into account radiation because of its minor contribution to the process. In this process the main heat transfer mechanism is conduction, although the air convection should be also considered in the analysis.

Conduction

According to [5] and [6], thermal conduction is the transfer of energy (heat) by microscopic collisions of particles and movement of electrons within a body. Conduction takes place in all phases of matte.

Heat conduction is caused due to a difference in the temperatures of two points of the work-piece. This difference, according to the principles of thermodynamics, causes a heat flow from the warm point to the cold point. Therefore, the rate at which

heat is conducted, is a function of this temperature difference (temperature gradient) between the two points and the properties of the conductive medium through which the heat is transferred:

$$\frac{\dot{Q}}{A} = -\lambda \frac{\partial T}{\partial x} \qquad (2.3.01)$$

λ is the thermal conductivity, $\dot{Q}$ is the heat flow, A the area through which the heat flows and T the temperature. This is the 1D-Fourier equation. It can be also written:

$$\dot{q} = -\lambda \nabla T \qquad (2.3.02)$$

The solution of this differential equation is $T(x,t)$, the temperature field.

The thermal conductivity is already calculated for many technical materials experimentally:

Material	$\lambda\ (W/mK)$
Cooper	382
Carbon steel	50
Aluminium oxide	30

Table 1: Values of thermal conductivity of some very used materials [6]

Convection

According to [5] and [6], convection is the heat transfer due to bulk movement of molecules within fluids such as gases and liquids. Convection cannot take place inside solids.

Considering a hot object surrounded by air, if the air moves, the object will cool faster than if the air was stopped. The intensity of the heat flow of this mechanism is proportional to the temperature difference between the object and the fluid. The proportionality factor α is called convection coefficient and depends on many other magnitudes of the fluid as well as its velocity, as α is bigger for a moving fluid than for a stopped fluid.

The heat flow density caused by convection is:

$$\dot{q} = -\alpha(T_s - T_f) \qquad (2.3.03)$$

T_s is the surface temperature and T_f the fluid temperature.

α is also calculated for different conditions and fluids:

Material	$\alpha(W/mK)$
Gas, natural convection	3-20
Gas, forced convection	10-100
Water, natural convection	100-600
Water, forced convection	500-10000

Table 2: Values of α of some very used materials [6]

Heating of a full cylinder

Temperature distribution

According to [3], the temperature distribution in a cylinder with a radius R and a constant power input $\wp_0$ is:

$$\Theta(r) = \frac{\wp_0 R}{\lambda}\left[2\tau + \frac{r^2}{2R^2} - \frac{1}{4} - 2\sum_{i=1}^{\infty} e^{\beta_n^2 \tau}\frac{J_0\left(\beta_n \frac{r}{R}\right)}{\beta_n^2 J_0(\beta_n)}\right] \qquad (2.3.04)$$

Θ is the temperature rise at r after the time t:

$$\tau = normalized\ time = \frac{\lambda t}{\gamma c R^2} \qquad (2.3.05)$$

With λ as the thermal conductivity. Eq. (2.4.04) can be rewritten in terms of the temperature rise compared to the temperature difference between the surface and the center of the cylinder. This is called normalized temperature:

$$\left[\frac{\Theta}{\Theta_s - \Theta_c}\right] = 2\left[2\tau + \frac{r^2}{2R^2} - \frac{1}{4} - 2\sum_{i=1}^{\infty} e^{\beta_n^2 \tau}\frac{J_0\left(\beta_n \frac{r}{R}\right)}{\beta_n^2 J_0(\beta_n)}\right] \qquad (2.3.06)$$

The $\sum$ term represents the transient rise, where $J_0(x)$ is a Bessel function of the first kind and zero order and the β_n are the positive roots of $J_1(\beta)$.

Figure 8 shows the normalized temperature $\Theta/(\Theta_s - \Theta_c)$ against the dimensionless radius r/R for various values of τ. Up to $\tau = 0.25$, the heat flow is in a transient state, with the temperature rising faster in the surface than in the centre. At $\tau = 0.25$ the transient finishes. Now the temperature distribution becomes parabolic. From now, the stationary begins, where all parts are heated at the same time, keeping the parabolic profile. By $\tau = 0.25$ the previous solution simplifies to:

$$\Theta = \frac{\wp_0 R}{\lambda}\left[2\tau + \frac{r^2}{2R^2} - \frac{1}{4}\right] \qquad (2.3.07)$$

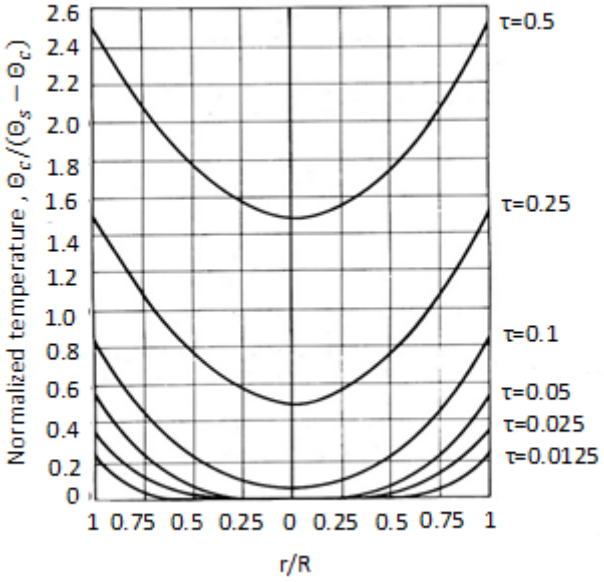

Figure 8: Temperature difference between the sides and the center of the rod for different times [3]

At the surface ($r/R = 1$) and at the centre, temperature is:

$$\Theta_s = \frac{\wp_0 R}{\lambda}\left[2\tau + \frac{1}{4}\right] \quad (2.3.08)$$

$$\Theta_c = \frac{\wp_0 R}{\lambda}\left[2\tau - \frac{1}{4}\right] \quad (2.3.09)$$

2.4 Surface hardening by induction

Metallurgical principles of heat treatment

According to [3] and [7], the most used material in induction heating is low-carbon steel. Figure 9 shows the equilibrium diagram for this material, in the concentration and temperature range interesting for this process.

At room temperatures, low carbon steel is has a body centered cubic structure (ferrite and cementite). At higher temperatures than ~723ºC, the microstructure starts to transform into face centered cubic structure (austenite) and the cementite dissolves into austenite. By increasing the temperature, more ferrite transforms into austenite until a fully austenitic microstructure is achieved. If now the work-piece is left cool slowly, the structure will change again to ferrite. Instead, if the piece is cooled rapidly enough, carbon atoms will not have enough time to precipitate from the fcc matrix and form cementite and gets enclosed in the body centered structure due to the phase transformation. The result is a super saturated body centered tetragonal structure, called martensite. Martensite stage consists of thin needle shaped grains,

which form a very hard crystalline structure. This process of rapid cooling is called quenching.

The rate of cooling is, therefore, a very important parameter. Is must not be below a critical value. The cooling is usually made using water in the form of sprays, especially for very low carbon steels, however in some applications oil is also used. Alloying the steel with alloying elements such as Mo, Cr, Mn and Ni can lower this critical value. The grade of steel, the cooling velocity, the previous metallurgical treatments and the coil design can affect the hardened depth.

One of the main advantages of induction heating is the high rate of power input and temperature rise, so steels that have high cementite solution rates in austenite are more suitable. This process has not the problems of through hardening like the incomplete transformation below the surface, because only the surface is heated. The centre of the piece retains its initial strength, obtaining then a piece with a ductile center and a hard surface. This is very suitable for pieces like gears, which are constantly receiving impacts when engaging

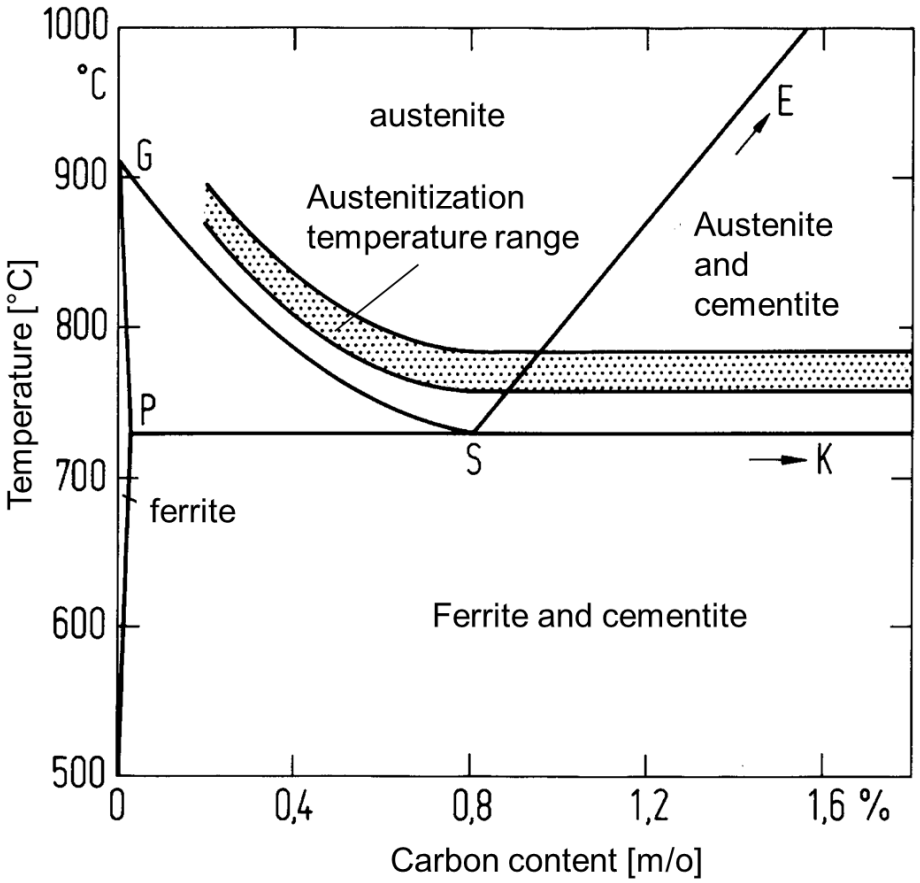

Figure 9: Iron-Carbon diagram for low carbon steels [8]

Typical hardening steels

The basis of selection of induction hardening steels is similar, but not identical, to the selection of hardening steels by other methods. An increase of the carbon content

results in increased hardenability. Also, as said, the addition of alloying elements such as Mo, Cr, Ni or W increases the stability of austenite, so that the ferritic and bainitic transformations are delayed. This results in improving the hardenability, i.e. the chance of getting austenite transformed into martensite by quenching under less extremely high cooling rates. Alloying enhances other important properties of the steel such as tensile, yield, impact and fatigue properties.
The amounts of carbon and alloy content suitable for induction heating are given in Table 3 in order of preference:

Carbon content (%)	Alloying element 1 (%)	Alloying element 2 (%)
0.35 to 0.6	None	None
0.3 to 0.4	Mn = 0.6 to 1.9	None
0.3 to 0.45	Ni = 3 to 5	None
0.35 to 0.45	Ni = 0.46 to 0.7	Cr = 0.3 to 0.6
0.35 to 0.45	Ni = 1.5 to 3.5	Mo = 0.25
0.35 to 0.45	Cr = 1	Mn = 0.6 to 1.2

Table 3: Carbon and alloy content suitable for induction heating [3]

Scanning quench

Quench is a vital part of the induction hardening process [3]. There are some types of quenches, but the ones interesting here are scanning quenches. Scanning quenches use a small coil to produce localized heat. The coil is moved along a cylindrical rod and the quench is applied immediately after heating. In this way, a small coil with relatively low power can be used to heat a large surface, at expense of the cycle of time. This process is illustrated in Figure 10. The coil, the quench ring and the work-piece are coordinated to give the best heating/cooling cycle. The quench ring sprays the cooler. The angle of spray is important: it must be used an angle up to 50° to obtain a more uniform cooling and some hardness depth.

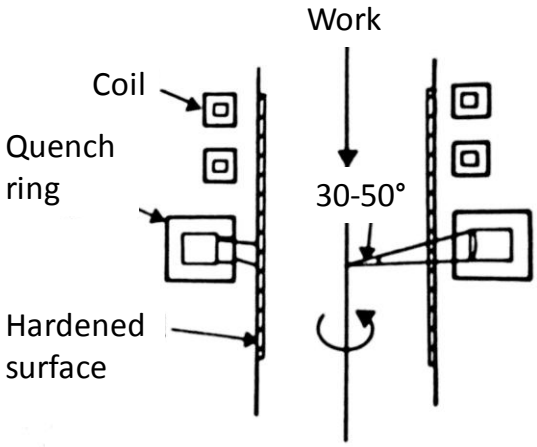

Figure 10: Illustration of scanning quench in a cylinder [3]

Selection of frequency

Many factors have to be considered in the choice of frequency for hardening. As said, high frequencies allow a more concentrated heating in the surface. Frequency must be chosen adequately to obtain the desired hardened depth.

Table 4 shows examples of frequency that is used in practice for induction hardening depending on the diameter of the rod and the hardened depth. This table should be used only as an indicator, as equally good results can be obtained by using lower frequencies and higher power density.

Hardened depth (mm)	Diameter of bar (mm)	Frequencies (kHz)
0.4-1.25	5-25	450
1.25-2.5	10-16	450 (10)
	16-25	10 ; 450
	25-50	10 (3 ; 450)
	Over 50	10 (3)
2.5-5	20-50	10 ; 3
	50-100	3 (1 ; 3)
	Over 100	1 (3)

Table 4: Selection of frequency in induction heating [3]

As we can see, the smaller the bar is, the higher the frequency should be.

3 Material properties

3.1 The 1.2344 steel and the 1.3505 steel

The steel that were used in the first two models is a 1.2344 steel. It is an alloy carbon steel that is normally used for tools. It provides a good balance between strength, ductility, high resistance to crack formation due to thermo-shock and good resistance for annealing. In the dilatometer model, a 1.3505 bearing steel was used. It is a low-alloy martensitic chrome steel. It has good characteristics of high hardness, resistance to wear.

The grade for these steel in other for other standarts organizations is detailed in Table 5, according to [9], [10], [11] and [12]:

Steel	SAE	EN (Number)	EN (Name)	JIS
1.2344	H13/T20813	1.2344	X40CrMoV51	SKD 61
1.3505	52100	1.3505	100Cr6	SUJ2

Table 5: Steel grades for 1.2344 steel and 1.3505 steel

Its approximated composition is detailed in Table 6:

Steel	Fe (%)	C (%)	Si (%)	Cr (%)	Mo (%)	V (%)	Mn (%)
1.2334	89.2-92	0.32-0,45	0.8-1.25	4.75-5.5	1.1-1.75	0,8-1.2	0.2-0.6
1.3505	98.4-98.85	0.95-1.1	0.35	1.3-1.6	0	0	0.2-0.5

Table 6: Chemical composition of 1.2344 steel and 1.3505 steel

They can also have small contents of Sulphur and Phosphorus.

Some of the typical applications of 1.2344 are:

- Extrusion dies for light alloys
- Shirts for extrusion
- Tools for die casting
- Hot cutting blades

Some typical applications of 1.3505 are:

- Balls for bearings and valves
- Automotive components
- Machine tools
- Pumps

3.2 Electromagnetic properties

Electrical conductivity

Electrical conductivity σ is the capacity of a material to conduct electric current [2]. Electrical conductivity depends on the disponibility of free electrical conductors in the material. The unit for electrical conductivity is the S/m:

$$S = \Omega^{-1} = \frac{A^2 \cdot s^2}{kg \cdot m^2}$$

There are four types of materials, depending on their ability to conduct electric currents through them: non-conductors, semi-conductors, conductors and superconductors. As metals are usually conductor materials, these will be the only considered here.

In conductor materials, the electrical conductivity decreases with rising temperature due to the increase of atom crashes that reduce the mobility of electrons. The variation of σ with temperature is shown in Figure 11.

Electrical conductivity is obtained from the definition of electrical resistivity ρ. The electrical resistivity describes the behaviour of a material against the passage of electrical current: a high value of resistivity indicates that the material is bad conductor while a low value indicates that it is a good conductor. The electrical conductivity is, therefore, the reciprocal of the electrical resistivity:

$$\sigma = 1/\rho \qquad (4.2.01)$$

For the both steels used, the electrical conductivity is:

$$\sigma_{1.2344} = 3.0303 \cdot 10^6 \ S/m$$

$$\sigma_{1.3505} = 4.6512 \cdot 10^6 \ S/m$$

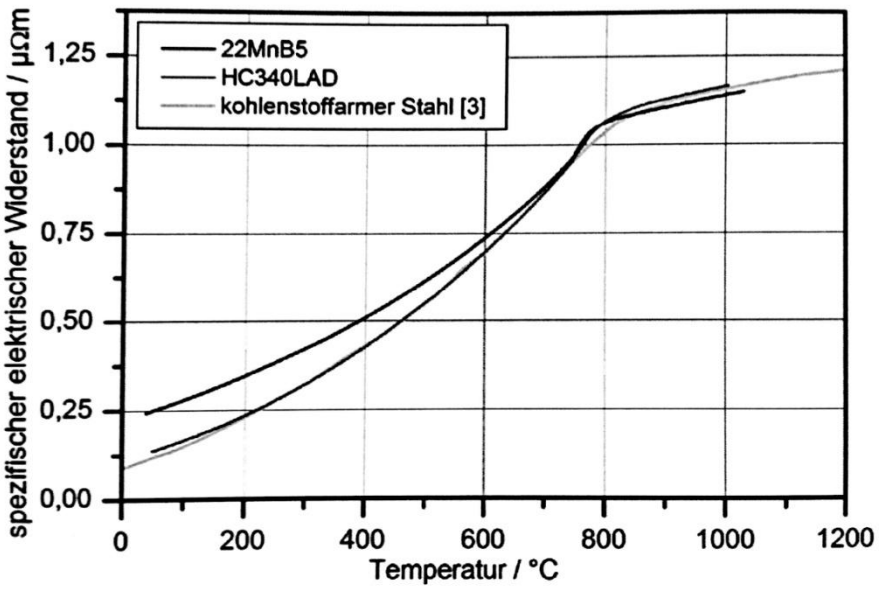

Figure 11: Variation of electrical conductivity with temperature [6]

Magnetic permeability

Magnetic permeability describes how easily the magnetic field passes through a material or how easily the material can conduct a magnetic field and is given by the relationship between the existing magnetic induction B and the induced magnetic field H [2].

$$\mu = \frac{B}{H} \tag{3.2.02}$$

It is usually represented as a dimenssionless relative magnetic permeability μ_r, which gives the relationship between the magnetic permeability of the material μ and the magnetic permeability in vacuum μ_0:

$$\mu_r = \frac{\mu}{\mu_0} \tag{3.2.03}$$

The magnetic permeability in vacuum is a known value ($\mu_0 = 4\pi \cdot 10^{-7} \frac{V \cdot s}{A \cdot m}$).

For ferromagnetic materials, the magnetic permeability depends on the temperature, decreasing with rising temperature. For the simulation, it will not be considered the ferromagnetic behaviour of the steel, hence:

$$\mu = \mu_0 = 4\pi \cdot 10^{-7} \frac{V \cdot s}{A \cdot m} \tag{3.2.04}$$

3.3 Thermal properties

Thermal conductivity

According to [5] and [6], thermal conductivity λ is a physical property of materials that measures the capacity of a substance to transfer the kinetic energy of its molecules to other adjacent or to one with which it is in contact. In a simpler way, it is the capacity of conducting heat through a work-piece because of the temperature difference between two points of itself. As defined in Eq. (2.4.02), the thermal conductivity is:

$$\lambda = \frac{\dot{q}}{|\nabla T|} \tag{3.3.01}$$

The units for thermal conductivity are W/mK.

The thermal conductivity of the steels is given for different for different temperatures in the following table.

	T=20°C	T=200°C	T=400°C	T=800°C
	Thermal conductivity in W/mK			
1.2344 [20]	19.32	23.57	27.41	26.05
1.3505 [21]	43,5	41,7	37,38	24,76

Table 7: Thermal conductivity of both steels for different temperatures

Specific heat capacity

The specific heat capacity is the amount of heat per mass unit that must be supplied to a system to raise its temperature by one Kelvin [5]. The specific heat capacity in conditions of constant pressure is represented with the letter c_p. The units for the specific thermal capacity are J/kgK.

It depends on the temperature. This dependence can be obtained with the following equation:

$$c_p = \lim_{\Delta T \to \infty} \frac{Q}{m\Delta T} = \frac{1}{m}\frac{dQ}{dT} \qquad (3.3.02)$$

Q is the heat transference between the system considered here and the environment, m is the mass of the system and ΔT is the temperature increase that the system experiences.

Usually, c_p increases with rising temperature, except in some monoatomic and diatomic gases. In Figure 12 is this dependence illustrated for carbon steel. The big change in c_p at 700 ºC is due to the change from ferrite to austenite.

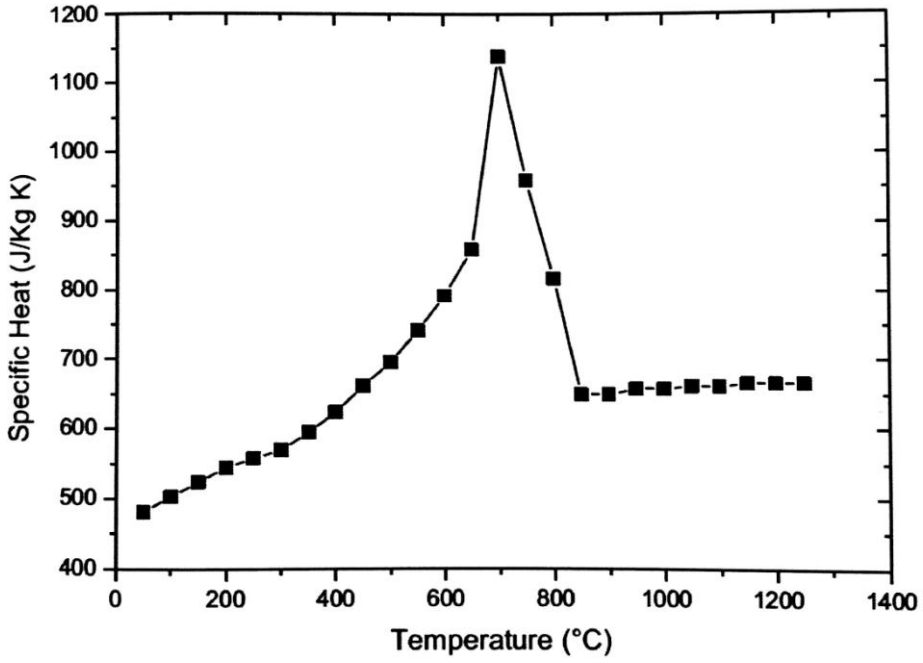

Figure 12: Variation of specific heat with temperature in carbon steel [6]

The thermal conductivity of the steels is given for different temperatures in the following table

	T=20°C	T=200°C	T=400°C	T=800°C
	Specific heat capacity in J/kg K			
1.2344 [20]	450	516	679	727
1.3505 [21]	440	544	621	615

Table 8: Values of specific heat of both steels for different temperatures

4 Introduction in the modelling of the induction heating in Abaqus/CAE

4.1 Description of the Finite Elements Method

Abaqus/CAE is based on the finite element method. According to [13] and [14], the finite elements method (FEM) is a general numerical method for the approximation of solutions of very complex partial differential equations used in various engineering and physical problems.

The method's procedure is divided in the following steps:

- Divide the region of the problem in a finite number of elements
- Select the interpolation functions, which will be used to approximate the values of the magnitude that we seek. The degree of this functions depends on the number of nodes of each element
- Define the elemental matrices and vectors of each element. These two form an equation system that relates the unknown values with known properties of the problem.
- Assemble the various elemental matrices and vectors to define the complete algebraic equation system. Also add the essential boundary conditions to the equation system.
- Solve the equation system. Form this phase it is normally used a computing program.

In this way, certain magnitudes can be calculated in a simple way, which in an analytical way would be very difficult to calculate. The accuracy of the method depends of the number of elements. The more elements that are used, the more accurate the method is. Due to the simplicity of the method, but also due the computing effort needed to solve it, this method is very appropriate for being used by computing programs.

4.2 Modelling in Abaqus/CAE

Modelling in Abaqus begins with the creation of the model. This model can be specified to three different types of simulations

- Thermal, mechanical and electrical analysis (Standard/explicit model).
- Fluid dynamics analysis (CFD model)
- Electromagnetic analysis

To build the model, one should create parts, assign sections with the corresponding material and assemble. The model should be meshed. The mesh is the division of the model with finite elements. The type, size and the number of the elements

depends on the analysis type and the process, being simulated. Having done this, the analysis type, e.g. heat transfer, mechanic, etc., are specified in the step module. To define the process, corresponding loads, boundary conditions and interactions with the medium are set. These loads, boundary conditions and interactions could have mechanical, thermal, chemical, electrical and magnetic nature.

4.3 Co-Simulation for induction heating calculation

Co-Simulation is a special type of analysis in Abaqus that is used usually to model complex multi physics problems with more than one analysis type. In the case of induction heating, the simulation begins with an electromagnetic model that calculates the eddy currents and the Joule heating generated by the electrical current in the coil. The second model is a Standard/Explicit model that calculates the heat transfer caused by the eddy currents.

The Co-Simulation does the analysis of both jobs at the same time by taking the results of the electromagnetic model into the heat transfer model, which calculates the heat flow and the temperature distribution.

To run a Co-Simulation it is necessary to create a configuration file, which connects the two jobs from the two models and defines the duration of the combined step [16]. At the time, the simulation cannot be submitted in the Abaqus graphical user interface. To run the Co-Simulation is necessary to introduce a special command in Abaqus command window, like the one showed in Figure 13.

```
abaqus cosimulation -j rod_emag,rod_heat -cosimjob
cosim -config rod_config.xml
```

Figure 13: Command for running the Co-Simulation

5 Objective

The objective of this project work is to build up a model for simulating the induction heating processes. The model is developed in the example of a cylindrical steel rod, being inserted in the variable magnetic field of an induction coil. The model should be used to study the correlation of the magnetic field, the induced current, the heating generated by Joule effect and the temperature distribution obtained with the process parameters, such as the frequency and electric current density, and geometrical effects depending on the position of the coil.

Finally, the feasibility of the electromagnetic and thermal Co-Simulation in Abaqus is evaluated by modelling the process of induction heating of a cylindrical sample in a quenching dilatometer, which is carried out at the thermophysics laboratory of IWM of RWTH_Aachen University.

6 Creating the models in Abaqus/CAE

Geometry of the model and material

The electromagnetic model consist of three parts: the rod, the coil and the air that surrounds the other two parts. These three parts will be merged in the assembly module into an individual part, which is used for the Co-Simulation . The part is named as *domain*. As shown in Figure 14, only a quarter of the cylinder is modelled based on the symmetry, in order to reduce the simulation time . The heat transfer model only consist only of the rod.

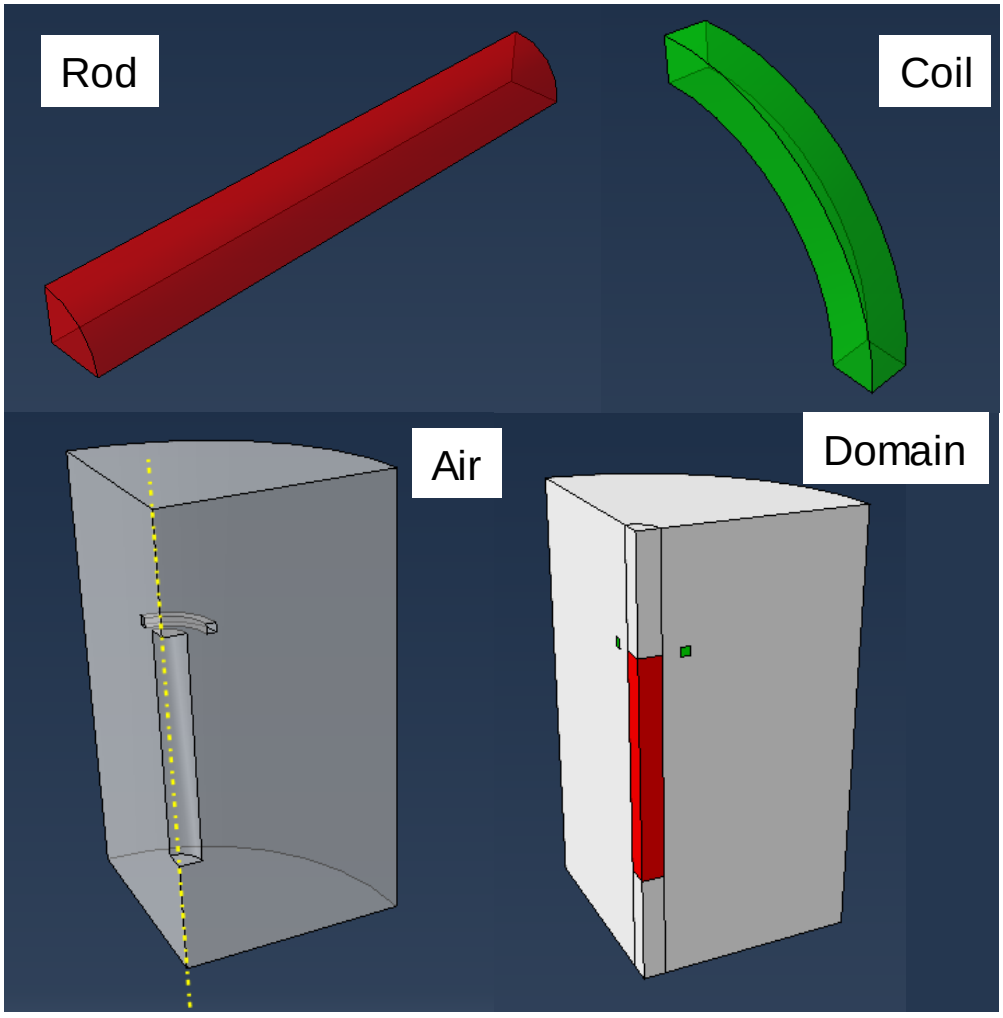

Figure 14: Parts of the electromagnetic model from Model 1: Rod (up left), Coil (up right), Air (down left) and Domain (down right)

The simulation has two different materials: *conductor* and *air*. *Conductor* represents the 1.2344 steel described in section 3. In the electromagnetic model, only the rod will be made of *conductor*, while *air* and *coil* will be modelled as *air.* The reason why the coil is modelled as *air* is because we are not interested in the heat and the

electromagnetic forces generated in the coil and we will assume that these are important in the analysis. *Air* has the following properties:

- Electric conductivity: $\sigma = 1000\ S/m$
- Magnetic permeability: $\mu \approx \mu_0 = 4 \cdot \pi \cdot 10^{-7}\ \frac{V \cdot s}{A \cdot m}$
- Convection coefficient: $\alpha = 10\ W/mK$

Thermal properties are not necessary, as *air* is not defined in the heat transfer model.

Mesh

The model was meshed with elements with corresponding degrees of freedom for the electromagnetic and the thermal analysis. The element types EMC3D8 and CD3D8 were chosen correspondingly. The size of the elements is different for the different parts, being smaller for the rod and the coil. That is due to the required accuracy of the results for the different parts. It is illustrated in Figure 16.

In the heat transfer model, the rod must have the same mesh, i.e. element size and number, and orientation in the coordinate system, so the results of the electromagnetic analysis could be transferred properly to the thermal analysis.

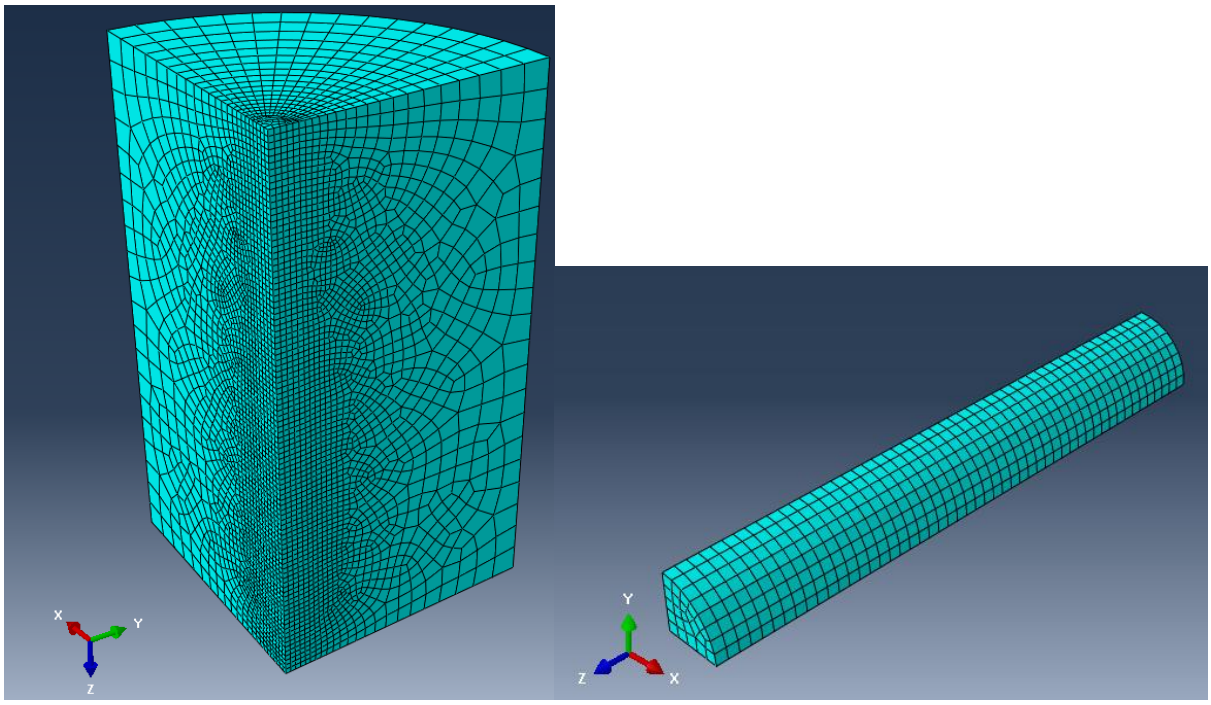

Figure 15: Meshes of the two models: electromagnetic (left) and heat transfer (right)

Process parameters

Frequency and step time

In both models it is necessary to define the step parameters. However, these are different for the two models.

In the electromagnetic model, the frequency of the feed alternate current was determined within the following range [6]:

$$5000\ Hz \leq f \leq 10000\ Hz$$

In the heat transfer model, the process time of induction must be set. The total time of was set to 120 seconds.

Electrical current (load)

Another main input parameter for the process is the power input. This is determined by the magnitude of the electrical current that flows around the coil. Figure 17 shows the current direction, defined in the induction coil as a load. The magnitude of the electrical current in the first two models will oscillate between two values:

$$4{,}5 \cdot 10^7 \leq J \leq 6.5 \cdot 10^7\ \ A/m$$

For the dilatometer model, higher electric current densities were used.

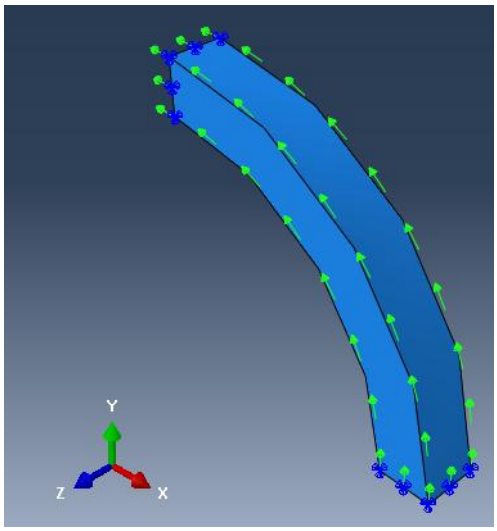

Figure 16: Load in the electromagnetic model: electrical current

Boundary conditions

The only boundary condition defined in the electromagnetic analysis was the magnetic vector potential, which was set to zero in all surfaces of the model.

Predefined field

The initial temperature of the rod was defined under predefined fields by $T_0 = 20°C$. If a sequence of steps is defined, the calculated temperature after each step defines the initial condition of the following step.

Interactions

The interaction with air was only defined in the heat transfer model. The interaction was defined as a surface film condition and represents the heat dissipation into the air by convection and radiation. It is defined by the convection coefficient α and the air temperature T_{air}. These two values will be:

$$\alpha = 10\ W/mK \quad ; \quad T_{air} = 20\,°C$$

6.1 Static coil model

This model represents the induction heating in the rod caused by one static coil. The induction was simulated for different positions of the coil along the rod to show the geometrical effect that causes different thermal conditions in the middle and in both ends of the part.

In Simulation 1, the coil was placed at one side of the coil, with only half of the coil surrounding the rod, while in Simulation 2, the coil will be placed surrounding the center of the rod, as shown in Figure 18.

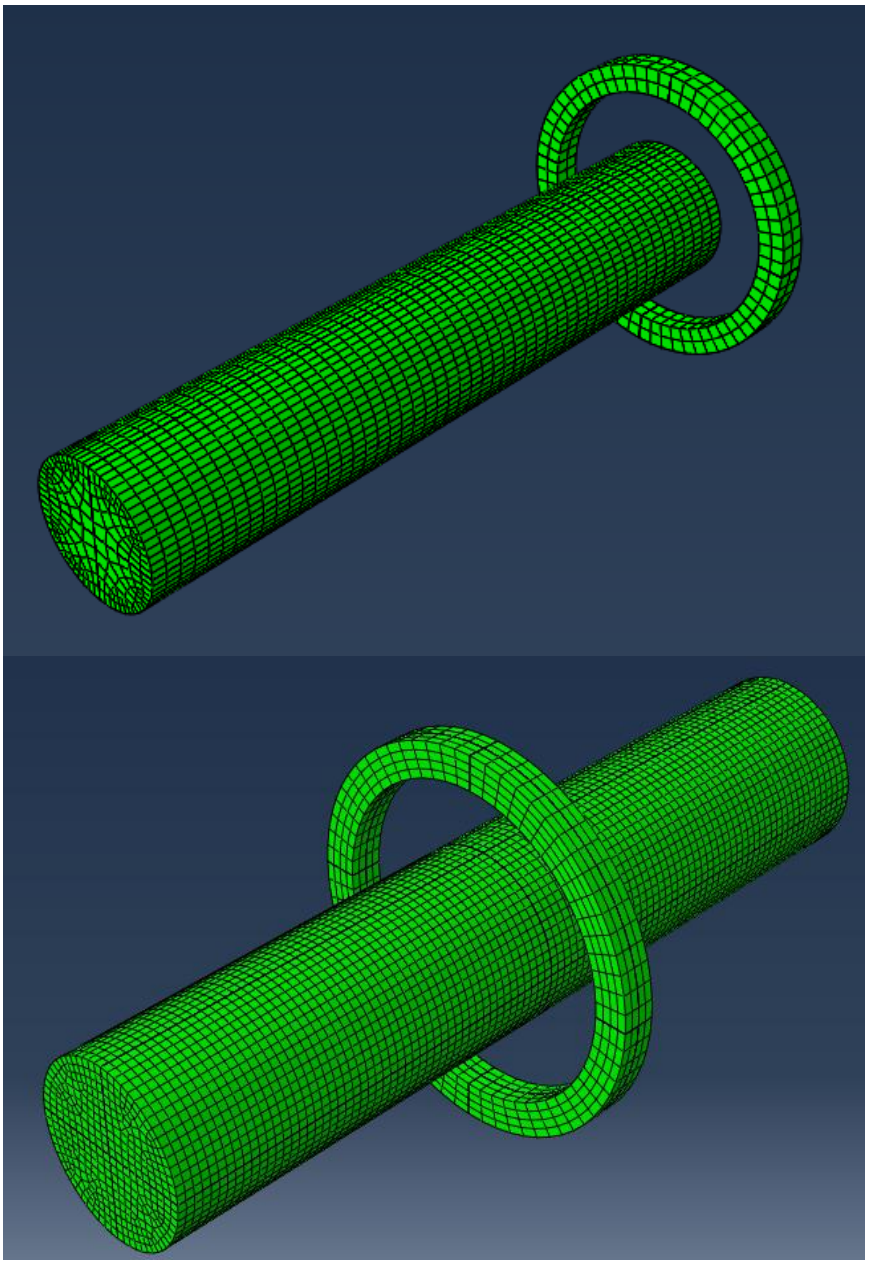

Figure 17: Simulation 1 (up) & Simulation 2 (down) (rod & coil)

This two models will show the difference between the heat transfer from one side and the heat transfer from the center.

6.2 Moving coil model

The induction heating of the full length cylinder was modelled by moving the coil along the rod. The coil could move along, either with a constant velocity or with a variable velocity. As Abaqus does not offer the possibility of simulating the direct movement of the coil, it was modelled by combining a sequence of Co-Simulations with static coils in different positions along the rod, being active for a certain time. The coils were placed in the simulation with equal distances, so the velocity could be

controlled by the step time. In order to let the coil move faster, the time was reduced correspondingly.

6.3 Dilatometer model

The last model was created to simulate the induction heating of a small cylindrical sample in the dilatometer of the thermophysics laboratory of the IWM. This process carried out consisted in three sequential heating stages from 20 to 850 ºC with different heating rates. The temperature was measured using two thermocouples, in the middle and at one of the ends of the sample.

Description of the laboratory device

This device consists of a chamber, inside which a hollow sample was heated by electromagnetic induction.

The device has the following components:

- 6-coil solenoid (1)
- 2 Aluminium Oxide subjections (2)
- Steel box (3)
- Vacuum generator (4)
- Hydraulic system (5)
- Electric generator (Not shown in the picture)

The dilatometer is shown in Figure 19.

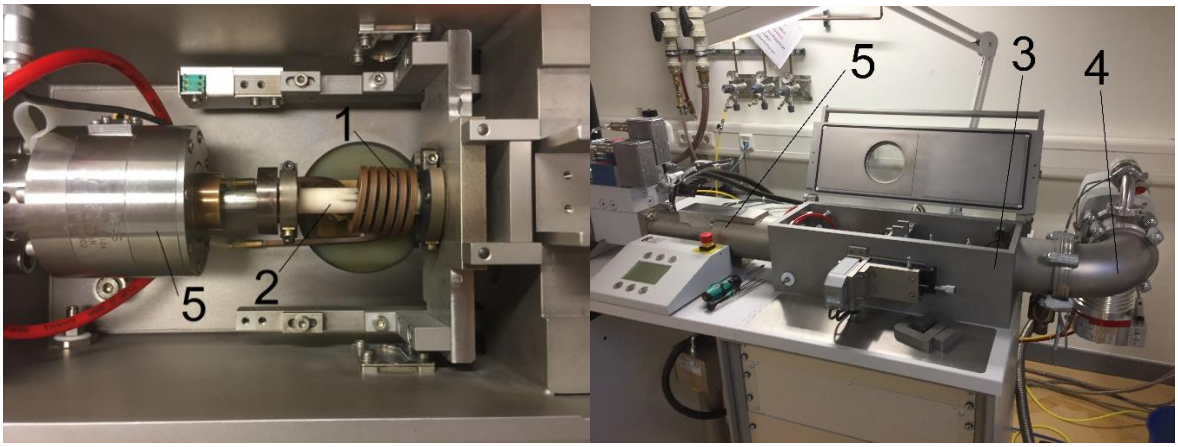

Figure 18: Laboratory device components

Before heating, vacuum is drawn to avoid oxidation of the sample at high temperatures. The desired temperature profile was programmed in the device special software by determining the temperatures and the heating time. The device software

uses the temperature measured by the middle thermocouple to control the cycle. Different heating rates are realized by controlling the frequency and power.

The rod had inner and outer diameters of $4\,mm$ and $2\,mm$ and a length of $10\,mm$, and was mounted between two stamps from aluminium oxide in a induction coil. The loads and the boundary conditions of the electromagnetic analysis are almost the same as in the previous models. The heat transfer model is quite different. The heat conduction from the sample to both stamps had also to be considered. Considering the vacuum in the chamber during heating, heat transfer by convection and radiation was neglected, being too small.

The properties of the aluminium oxide (Al_2O_3) are the following [15]:

- Thermal conductivity: $30\ W/mK$
- Specific heat: $850\ kJ/kgK$
- Density: $3900\ kg/m^3$

In Figure 20, the model for the dilatometer tests is illustrated.

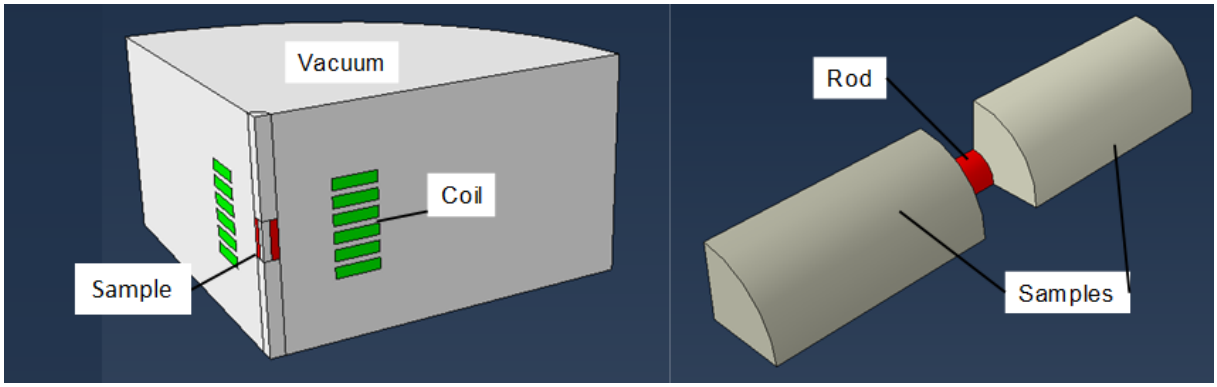

Figure 19: Model for the electromagnetic analysis, including induction coil, sample and air (left) and model for the heat transfer analysis, including the sample and the stamps (right) of Model 5.

7 Results of the simulation

7.1 Influence of process parameters in the static model

In this section, it will be shown how the different process parameters affect the temperature distribution in the rod. These parameters are the input of the process that can be controlled.

Frequency

Frequency is one of the main parameters that is usually used to control the heating in the work-piece. This frequency corresponds to the oscillating frequency of the feed alternate current of the coil.

The different temperature distributions was obtained using six different frequencies $(5000, 6000, 7000, 8000, 9000 \,\&\, 10000\ Hz)$ for a total time of 120 seconds with a constant current J

$$J = 4{,}5 \cdot 10^7\ A/m$$

The form of the temperature distribution in the rod for Simulation 2 is shown in Figure 21:

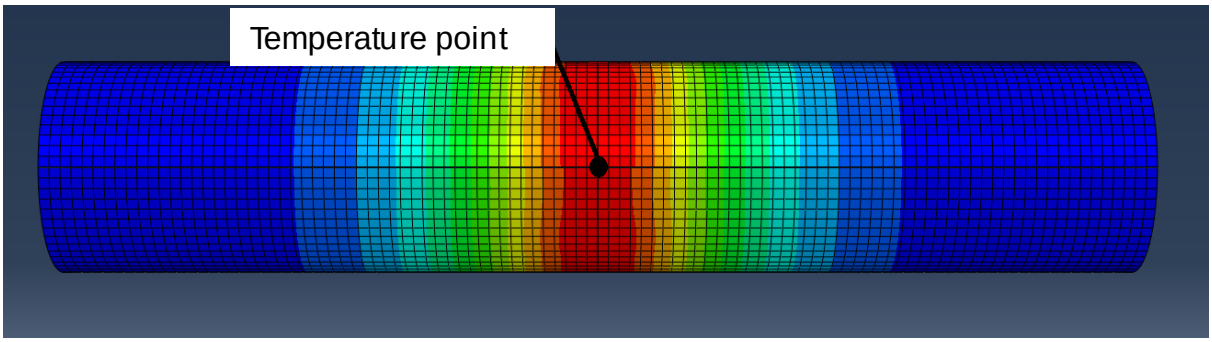

Figure 20: Form of the temperature distribution in Model 2 and temperature point for the comparison (black point)

To see the differences in the temperature, the temperatures in one point of the rod will be obtained for the different frequencies. This point is also displayed in Figure 21.

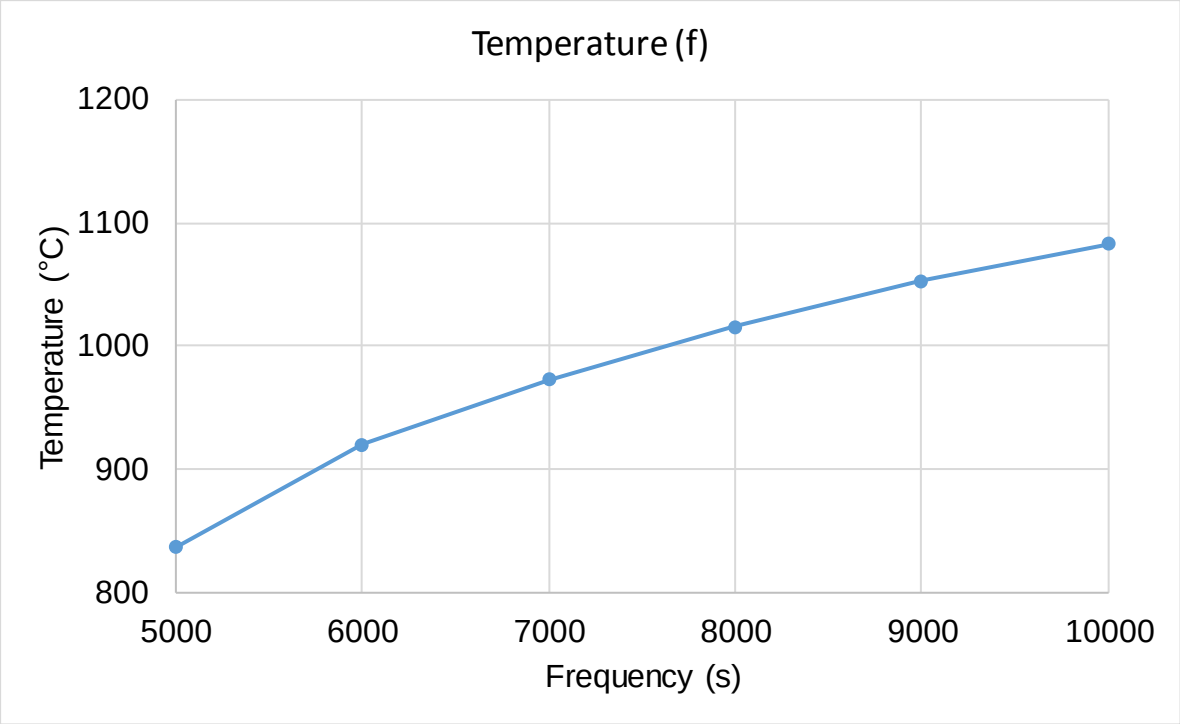

Figure 21: Relationship between Temperature (°C) and frequency (Hz)

As shown in Figure 22, temperature grows with increasing frequency, but following a degressive relationship. With this results, it can be deducted that for low frequencies, frequency can be used in this case as an input parameter, but for higher frequencies, the variation of the temperature in the center of the rod will become smaller the higher the frequency is. Therefore, this parameter will be better to control the process in the range of low temperatures.

Electric current density

As in the previous section, the temperature distribution will be obtained, but this time depending on the power input. Power input is controlled by changing the electric current density, which has the following proportional relationship with the power:

$$P \propto J^2$$

This time, the frequency of the simulation will be a constant value of $5000\ Hz$ and the current density will change. For the current density, there are 4 different values. The induction time, as in the previous section, will be 120 seconds. Also the temperature point will be the same as previously.

The following figure shows, the different values of temperature for the different current densities.

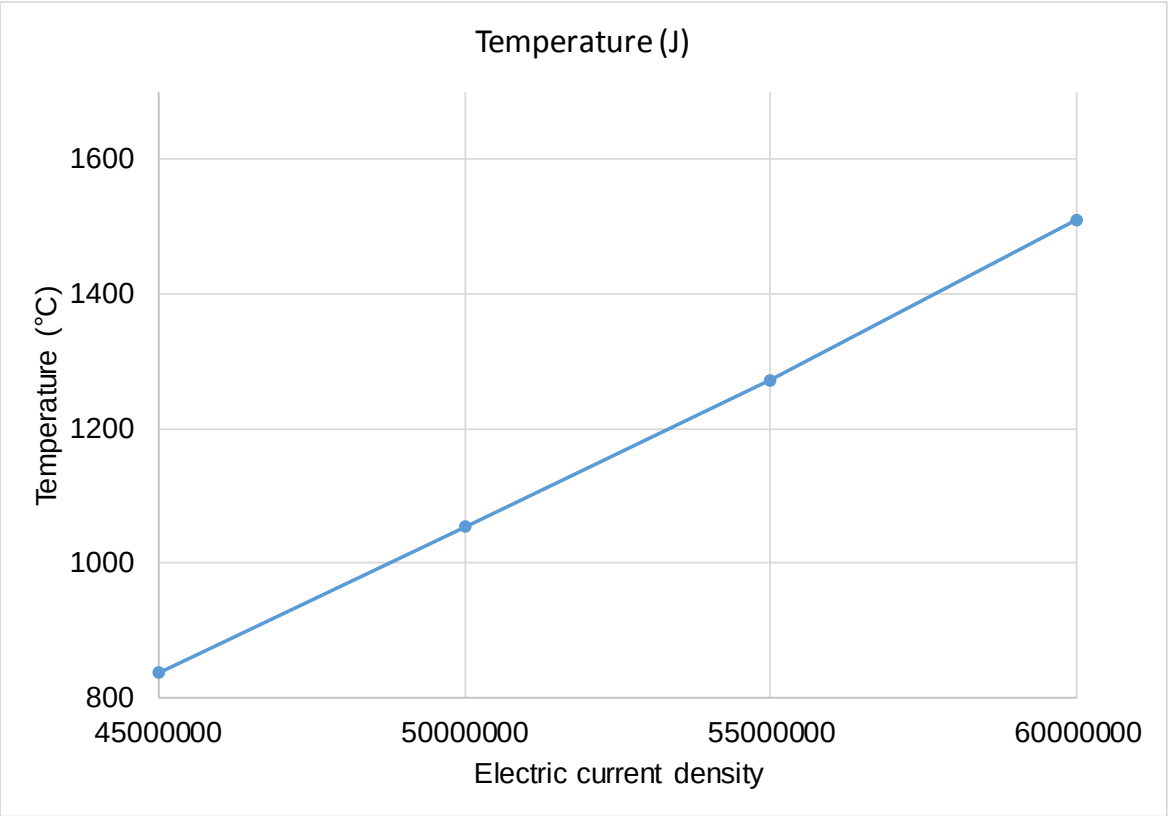

Figure 22: Relationship between Temperature (°C) and electric current density (A/m)

As shown in Figure 23, temperature grows with rising electric current density, following a second degree function, but almost linear. This is because temperature and power input are directly proportional, as explained in section 2.1.
By combining the effect of both parameters, the work-piece can be heated to a very wide range of temperatures in the center of the rod. For example, to heat the work-piece to a very high temperature, a constant high frequency can be set and the electrical current density used as main input parameter to get to the desired temperature.

Time

In this section it will be shown how the temperature grows along the 120 seconds of heating. Process time is another main input parameter.
By establishing constant values for the frequency and for the current density, the parameter that allows to control the heating is time. However, this parameter, in general, is not as important as the previous two, since high frequencies and powers are often used to heat the piece very quickly and thus minimize the heat conduction towards the center of the piece. Even so, it is important to know how the temperature grows over time throughout the heating. The temperature point will be the same as in the previous sections. The frequency and the electrical current density will be the minimum from the previous sections ($5000\ Hz$ and $4{,}5 \cdot 10^7\ A/m$ respectively).

A linear relationship between time and temperature is obtained, although the first part of the temperature rise is not linear due to the transitory. This is displayed in Figure 24.

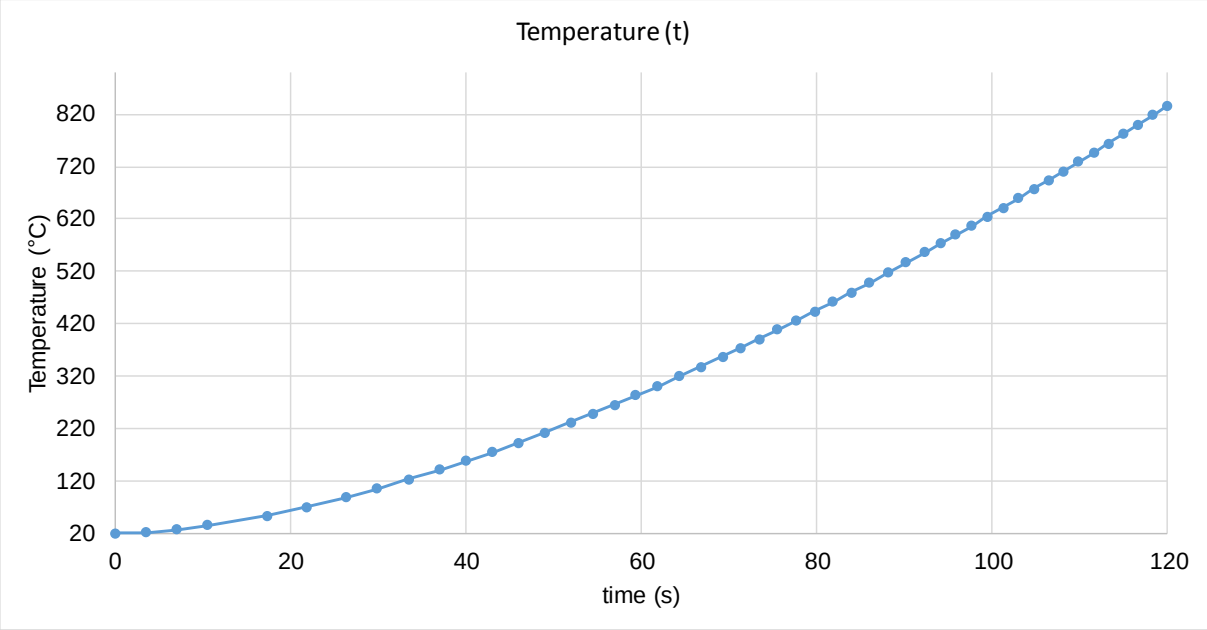

Figure 23: Temperature growth (°C) throughout the heating time (s)

As shown, the heating increases with time, therefore, care must be taken with the time not to overheat the work piece. This can cause grain growth and melting of the work piece if the heating does not stop. Time is an important input parameter in case of having a small electric generator without access to very high electrical currents and frequencies.

Position of the coil in the z-Axis

The position of the coil along the rod is very important for the heating process. Besides that the coil specially heats the region close to itself, as the eddy currents in this area have their maximal value, the maximum temperatures in the center and in the sides are not the same for the same heating parameters. The reason for this is the different distribution of the eddy currents in both positions. As explained, eddy currents flow in closed loops perpendicular to the magnetic field, whose direction is the z-direction. Therefore, the eddy currents in the center flow around the rod, specially concentrated at the surface. Meanwhile, in the sides, as only half of the coil covers the rod in this position, the eddy currents are more concentrated in the base of the rod, causing a higher heat by Joule effect there.

Despite there is also heat convection, it is small compared to the conduction because it is natural convection and not forced convection. Conduction is the main heat transfer mechanism in this simulation. It was considered that conduction in other

directions apart from the z-direction is also to be neglected, due to the dimensions and form of the rod.

By placing the coil in the center, once it starts to heat the rod, the heat is conduced to both sides of the rod, which are colder that the center. Instead, by placing the coil at one side, the heat can only be conducted to one side and, therefore, the peak temperature is much higher in this case. In the second case, the heated zone is also smaller than in the first one, which means that the heat is more concentrated in this case. These differences are shown in the temperature distribution in Figure 25.

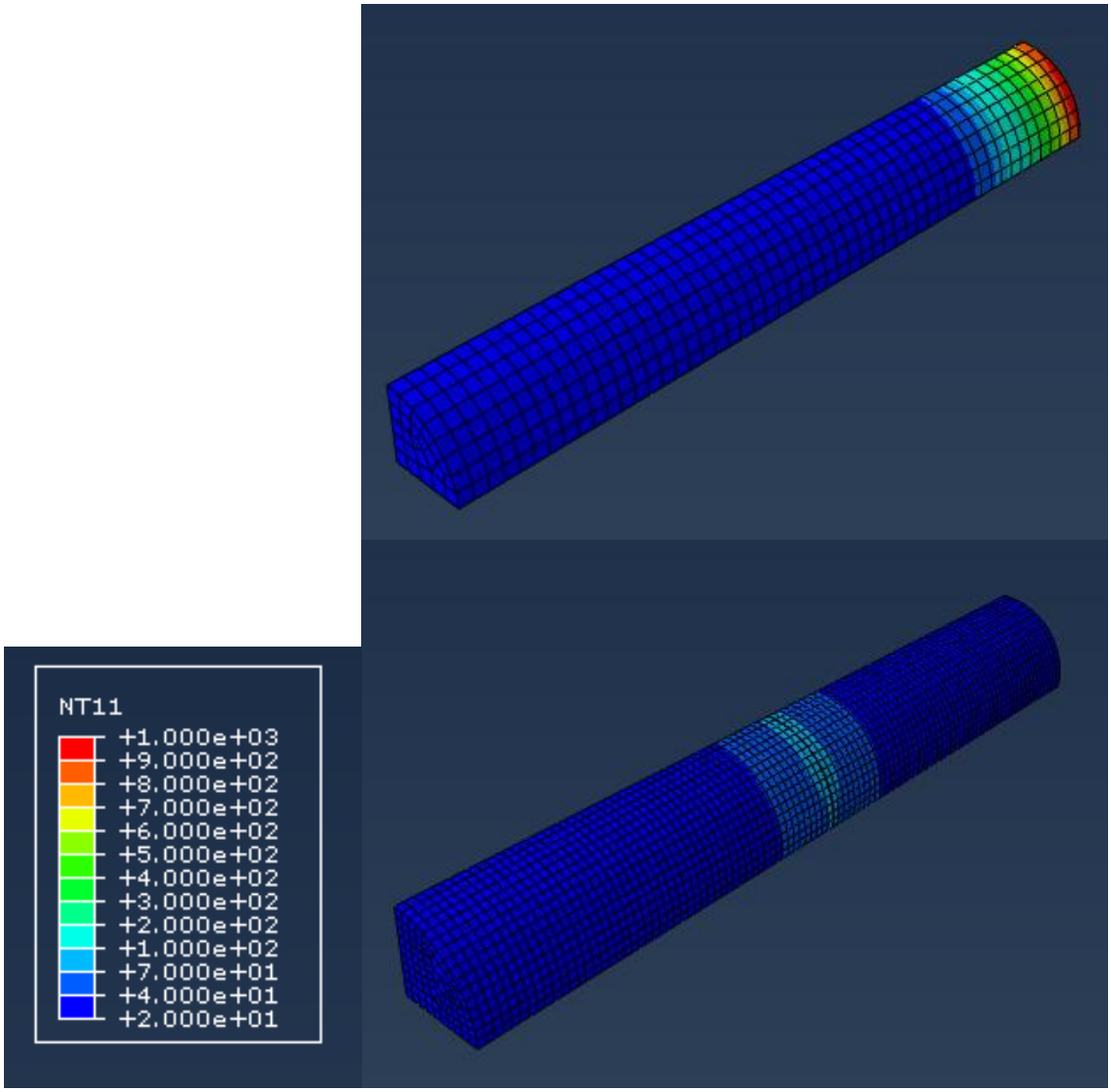

Figure 24: Temperature distribution in Model 1 (up) and 2 (down)

The other process parameters are the same for both simulations:

$$J = 4{,}5 \cdot 10^7\ S/m \quad ; \quad f = 5000\ Hz \quad ; \quad t_{max} = 22\ s$$

As shown, the maximum temperature at the end is much higher than in the center. Both peak temperatures are:

$$T_{peak,1} = 985{,}48\ °C \quad ; \quad T_{peak,2} = 73{,}05\ °C$$

Care must be taken when heating the sides of the rod, because if, like in this simulation, the same process parameters are applied to both positions of the coil, the ends of the rod can be melted in the worst case. The ends must be heated less time than the center to avoid this. This is the reason why in the moving coil model a variable velocity to the coil will be applied.

Proximity of the coil

The proximity of the coil to the rod is another parameter that should be taken into consideration. As explained in the proximity heating section, the closer the coil is, the higher the temperature gets. Also, due to the proximity of the coil to the rod, we can consider the current through the coil as a line current at a distance h from flat plane. h will be in this case the distance from the surface of the rod to the center of the coil.

To simulate this, we use Model 2 with the following process parameters:

$$J = 4{,}5 \cdot 10^7\ S/m \quad ; \quad f = 5000\ Hz \quad ; \quad t_{max} = 120\ s$$

The temperature for the different values of h are displayed in Figure 26:

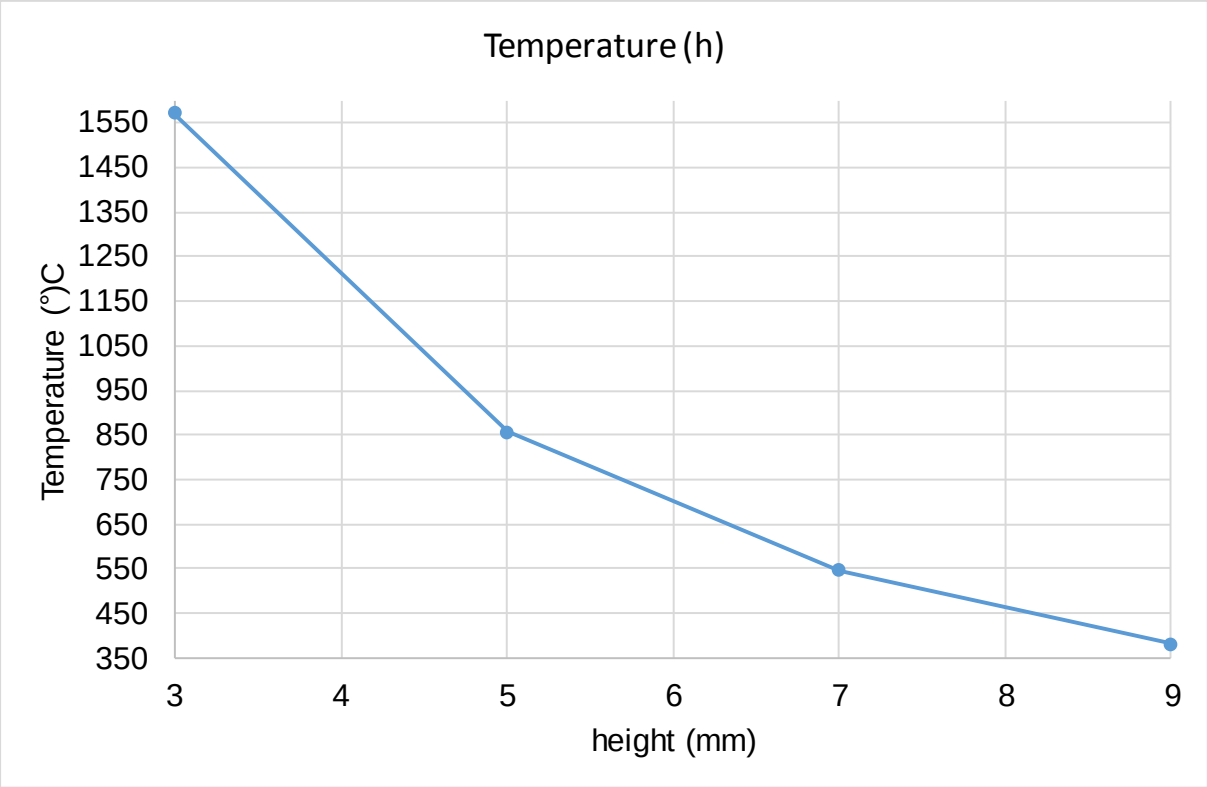

Figure 25: Relationship between temperature and the distance of the coil h

As shown in the figure, temperature grows a lot by putting the coil very close to the rod. The power input rate follows an inverse function, like in Eq. (2.1.16), which means that the temperature, that is proportional to it, will also follow this function.

This parameter can be interesting if a only weak electric generator is available, as the temperature can get very high without using high currents or frequencies. Care must also be taken when putting the coil to avoid heating the rod too much, because, as shown in the example, the surface of the rod can be easily melted.

7.2 Influence of process parameters in the moving coil model

Constant velocity simulation

In this simulation, the temperature evolution along the heating caused by a moving coil is analyzed. This coil moves with a constant velocity.

To simulate this, as Abaqus has not the option to directly simulate the movement of the coil in a transient heating, the simulation was divided in five sequential sub-simulations. Each of these consist in a static coil placed at different positions along the coil, starting from one of the ends of the rod. After each one, the following sub-simulations take the temperature distributions at the end of the previous ones as a temperature predefined field. Each of these sub-simulations lasts an equal part of the total heating time, which is 120 seconds. Therefore, each simulation has a step time of 24 seconds. The frequency and the electric current through the coil are constant during the five sub-simulations. The values of the process parameters are:

$$J = 4{,}5 \cdot 10^7\ S/m \quad ; \quad f = 5000\ Hz \quad ; \quad t_{total} = 120\ s \quad ; \quad t_{step} = 24\ s$$

The velocity of the coil that was approximately simulated is:

$$v = \frac{l_{rod}}{t_{total}} = \frac{0{,}05}{120} = 4{,}17 \cdot 10^{-4}\ m/s = 0{,}417\ mm/s$$

The proximity of the coil will be the same as in the static model.

With this model, it will be studied how the temperature changes along the total heating time for the different positions of the coils and the difference between the temperatures in different points of the rod.

Temperature evolution along the time

For this case, it will be shown how the temperature changes along the total time of heating in two different points of the rod. These points will be placed at the center of the rod and at one of its ends. It will be also shown the big difference between the two maximal or peak temperatures, as explained in the previous section.

The two peak temperatures in each point are:

$$T_{peak,end} = 1148{,}21\,°C \quad ; \quad T_{peak,center} = 524{,}58\,°C$$

These peak temperatures are reached in the first sub-simulation for the one in the ends and in the third simulation for the one in the center. As shown, there is a big difference between the two temperatures, due to the different heat conduction and magnetic field distribution and, therefore, eddy currents in these two points, as explained in the previous section.

Figure 27 shows the temperature evolution along the time for the two points.

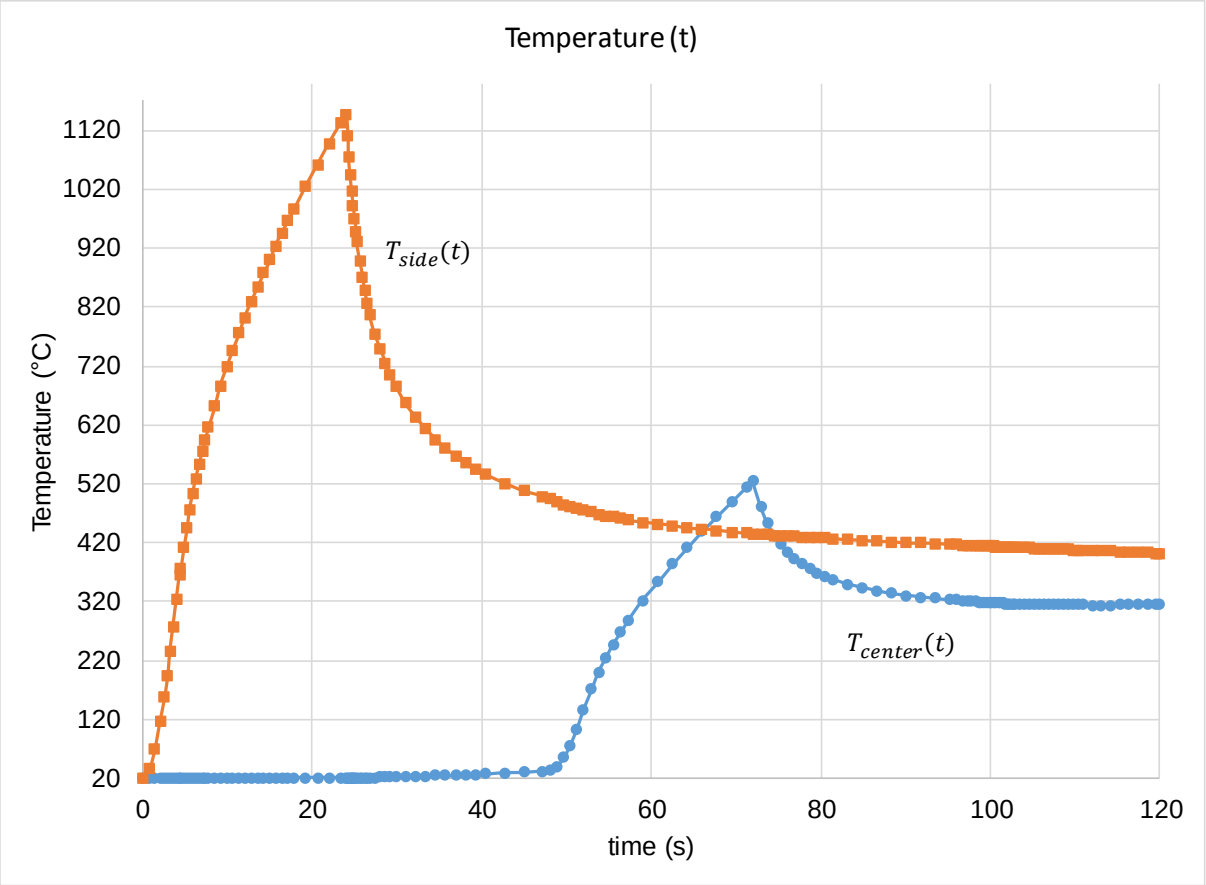

Figure 26: Temperature evolution along the time

As shown in the figure, the temperature at the side grows quickly to its peak value at the end of the first sub-simulation (24 seconds). After this, the temperature decreases also quickly because of the heat conduction caused by the big temperature difference between the end and the rest of the coil. The rate of temperature fall decreases with time and, approximately by 500°C, the temperature fall rate is already small. The temperature does not decrease more because of two reasons:

- The heat conduction in this material is not very high because of the small thermal conductivity of this steel, compared to other steels.
- When the first coil stops the heating, the second one starts, increasing the temperature in the second area of simulation. This reduces the temperature difference between both areas, reducing also the heat conductivity.

The end temperature after the second simulation stays in a more or less constant value of 420 °C due to the second reason explained previously. On the other hand, the center temperature does not grow a lot during the two first simulations. The heat conduction contribution is approximately equal to the air convection contribution during the first 45 seconds. After this, the heat conduction starts to increase due to the increasing difference of temperature between the center and the area of the second simulation. When the third simulation starts, temperature grows much faster, reaching the peak temperature at 72 seconds. After the third simulation, temperature decreases in a similar way to the temperature at the end of the rod, although at a lower speed, since the difference in temperature between the center and the surrounding areas is lower than in the first case.

With the final temperatures that were obtained here is impossible to harden the rod, since the austenite temperature is around 750 °C.

Peak temperatures along the rod

As obtained in the previous section, the maximal temperatures in the rod for by using a constant velocity of the coil are quite different depending on its positions along the rod. This is due to the different heat conduction that is possible depending on the position.

In Figure 28, the peak temperatures for the five sub-simulation points are shown. The reference point for the position is the end of the coil, where the first sub-simulation is done.

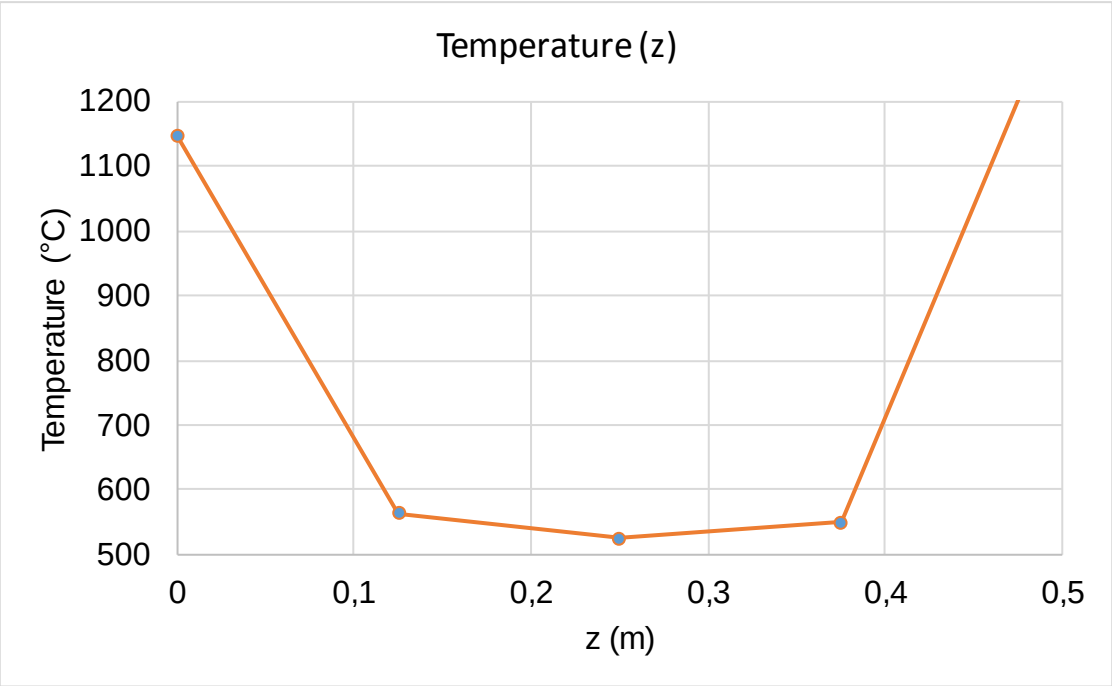

Figure 27: Peak temperatures (°C) for the different positions along the z-axis

Figure 28 shows that both temperatures at the ends are much higher than in the center. The temperatures in the points between the ends and the center are also higher than the one in the center, but only a few. There is also a difference between the two peak temperatures at the sides and the two form the medium points.

- The slight difference between the temperatures in the medium points is due to the different heat conduction they receive from their previous stages of the simulation. The one at $z = 0{,}125$ receives the heat conduction from the heating of the first side, whose peak temperature is more than 1000 °C. This conduction, as shown, is quite high in the first moments of sub-simulation 2. Meanwhile, the point at $z = 0{,}375$ receives the heat conduction from the third sub-heating, the one in the center. This one has a peak temperature of 524,58 °C, which means that the heat conduction will not be that intense. This difference causes that both points start their respective heating processes at a different initial temperature. However, the difference is slight because this heat conduction contribution is not very high compared one of the heating by induction.
- The difference in the peak temperatures at the sides is caused by the same effect, but in a different manner. In this case, the first side starts with a uniform temperature in the whole rod of 20°C, while the last one has received heat conduction from all the previous stages. This causes that the last point starts its simulation already with 150 °C.

The temperature distributions at the instants of peak temperature (end of each simulation) are shown in Figure 29.

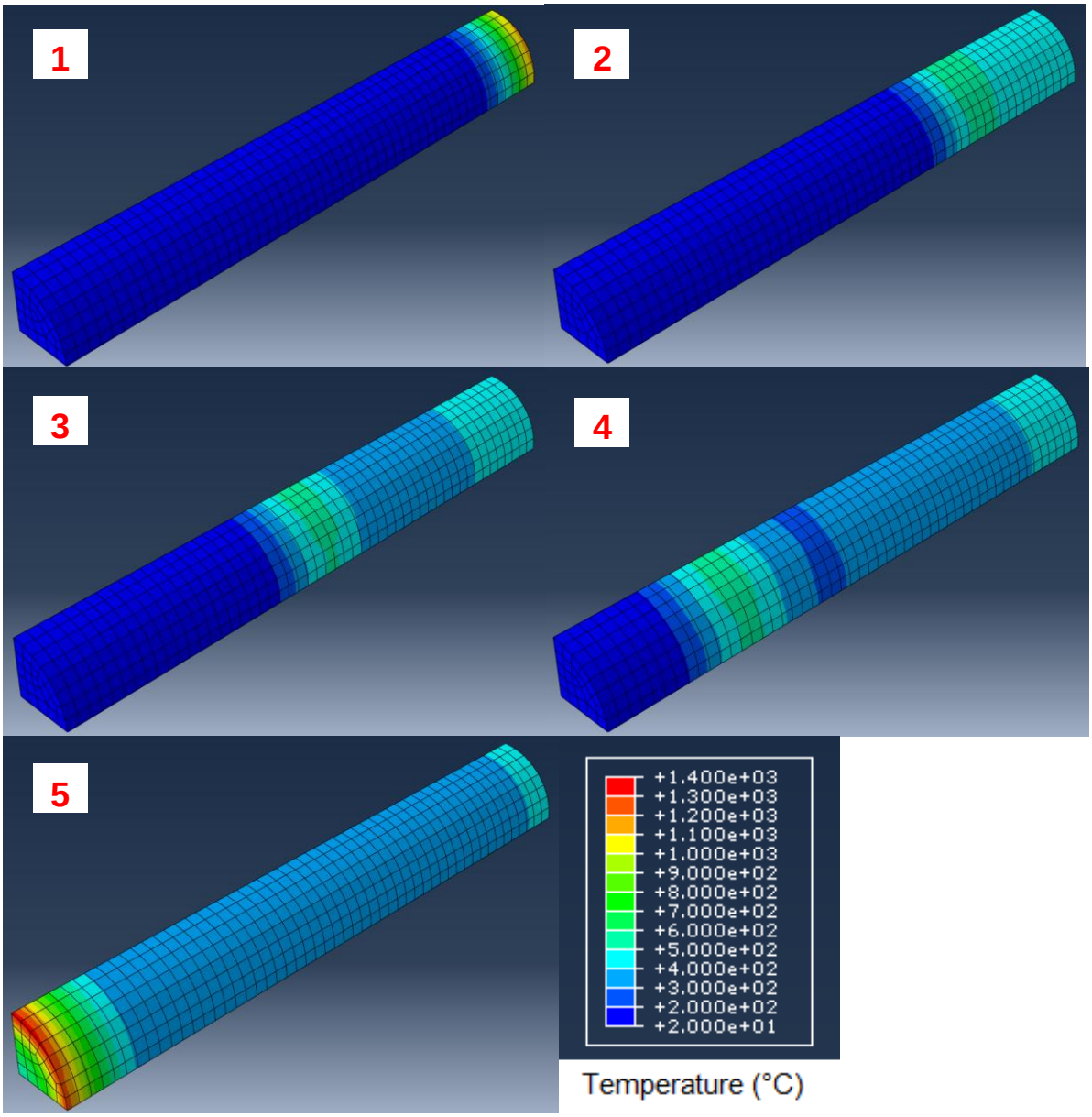

Figure 28: Temperature distributions at the end of each simulation and temperature legend

Variable velocity simulation

This simulation was made mainly to solve the problem of the big difference between peak temperatures along the rod. To solve that, instead of using a coil that moves with a constant velocity, a coil whose speed changes depending on how fast each part of the rod has to be heated is used. This way, the rod can be heated in its different areas just to the necessary temperature and immediately quench it, so almost no grain growth along the rod is obtained.

This simulation consist in 10 sequential sub-simulations and follows the same principle of defining the temperature predefined field as the previous temperature distribution as the previous model. The difference here is that the simulation steps do not last the same time.

The process parameters are the following:

$$J = 6{,}25 \cdot 10^7\ S/m \quad ; \quad f = 5000\ Hz \quad ; \quad t_{max} = 91\ s$$

Position and velocity of the coil (Step times)

The variable velocity in this model is simulated with the different step times of each sub-simulation. Starting from the problem of the difference in peak temperatures, the ends are heated faster than the center. Knowing this, the coil speed has to be high on the ends, while being lower in the center.

However, if the sides are heated very fast, the adjacent area could not be heated enough. Therefore, the velocity right after the side should be a bit lower than the one in the center. It should be also taken into account that, in the second half of the simulation, the simulation areas will receive more heat conduction from the previous stages and, therefore, their initial temperature will be higher, which means that the velocity in the second half should also be higher. This can be accomplished by using a fourth degree function, for example.

The positions of the coil throughout the total time are displayed in Figure 30.

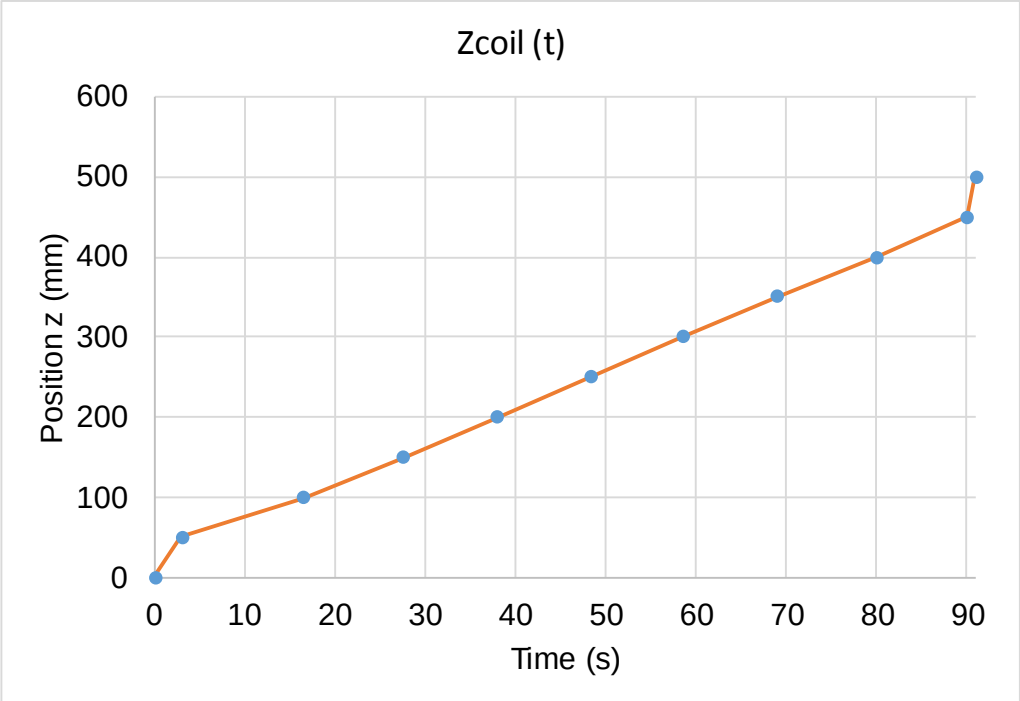

Figure 29: Position of the coil (m) along the time (s)

As the figure shows, the position of the coil in the real process can be approximated with a fifth degree function. Hence, the speed of the coil will follow a fourth degree function. The position function can be obtained from the points of position and the time. By doing this, the following approximate expression for the position is obtained:

$$z_{coil}(t) = 1{,}27 \cdot 10^{-6}t^5 - 3.057 \cdot 10^{-4}t^4 + 0{,}027t^3 - 1{,}023t^2 + 19{,}5t\ (mm) \quad (8.2.01)$$

By derivating, the speed is obtained:

$$v_{coil}(t) = 6.36 \cdot 10^{-6}t^4 - 1.22 \cdot 10^{-3}t^3 + 0.0804t^2 - 2.0458t + 19.5\ (mm/s) \quad (8.2.03)$$

The velocity of the coil is displayed in Figure 31 [15].

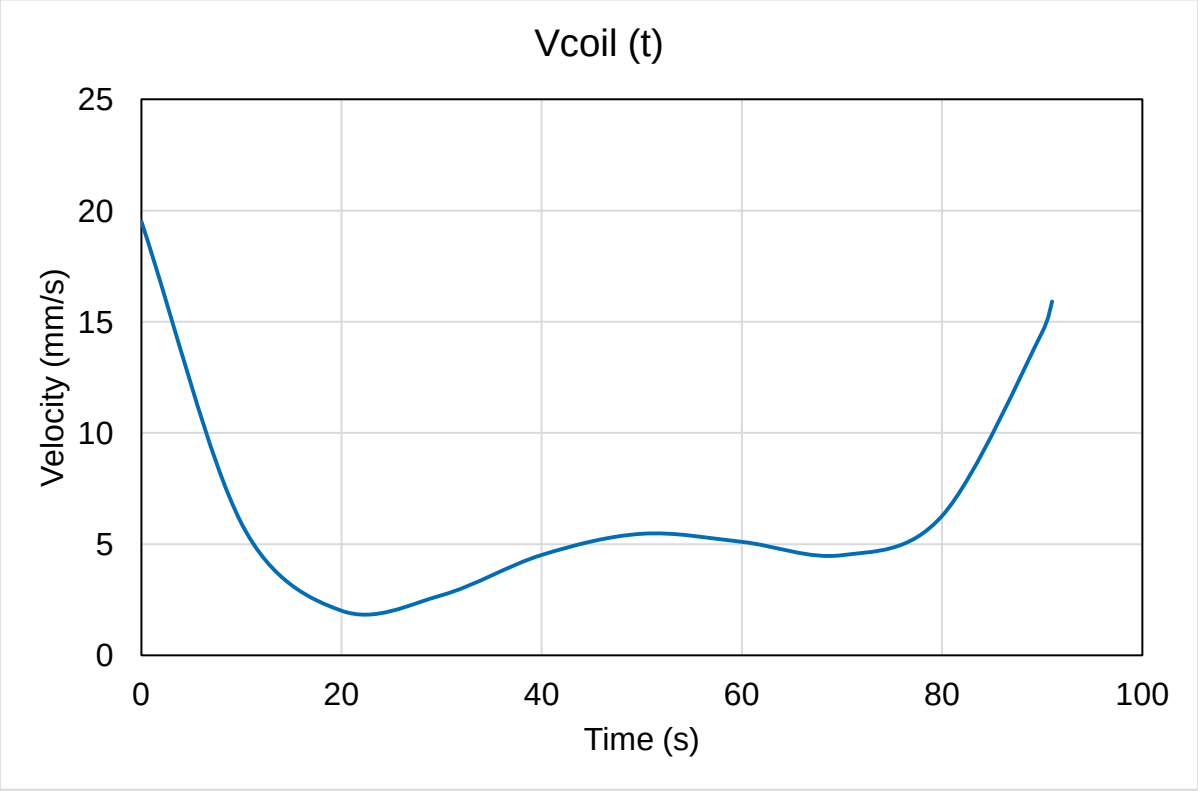

Figure 30: Velocity of the coil with time

Temperature evolution throughout the total time

As in the constant velocity simulation, it will be shown how the temperature changes during the whole process time. In this case, the differences in the evolution of temperature are obtained for three different points of the rod. These three points are shown in red in Figure 32.

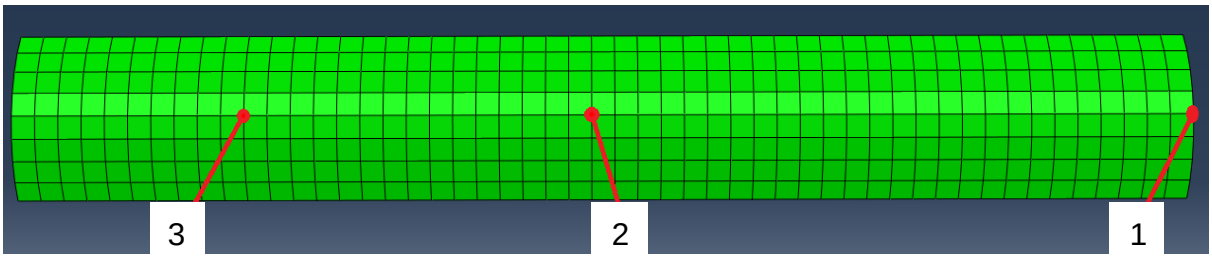

Figure 31: Points for the analysis

The evolution of the three temperatures in this case is displayed in Figure 33.

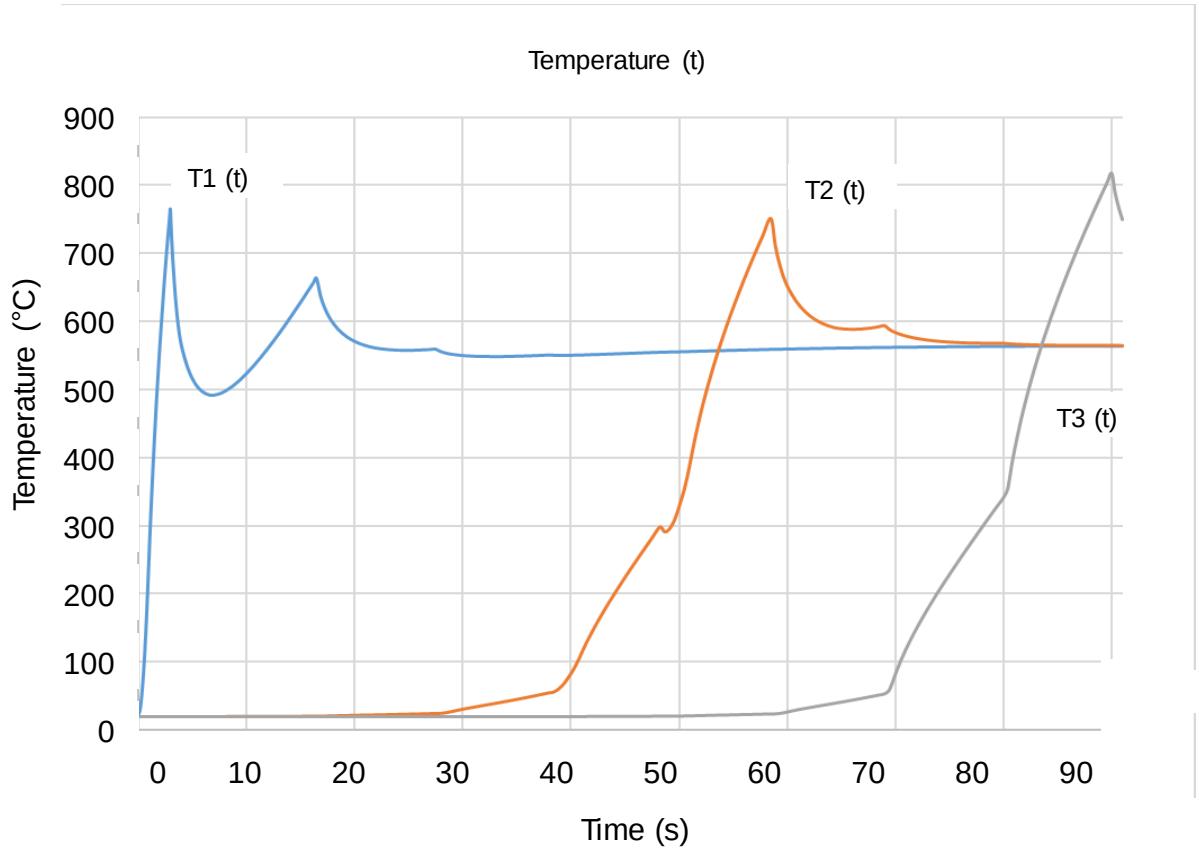

Figure 32: Temperature evolution in the three points

The figure shows that, in this case, a very similar temperature evolution for point 1 as in the previous model is obtained. The difference is that the temperature only reaches to almost 800°C, instead of the 1148°C from the previous simulation, due to the very short step time for the sides (3 seconds).

The second temperature peak is higher than that of the previous model and this time it reaches the austenitization temperature. This was achieved with a long heating in the center, which lasts 20,5 seconds between the two center coils (Coil 5 and 6) and especially because, in this model, a higher current density J was used.

Point 3 shows a similar heating as the one of point 2, but with higher temperatures, as the area starts the heating with a higher initial temperature. This first temperature increase (until 80 seconds) is due to the conduction along the process.

Peak temperatures along the rod

From the results of previous section, the peak temperatures now are more uniform in the center due to the precise heating in all areas. In this simulation, the velocity of the coil is a more important parameter than the heat conduction, although it cannot be neglected.

In Figure 34 are displayed the peak temperatures after the corresponding heating for each one of the 10 coil positions. The reference point is the same as in the previous model.

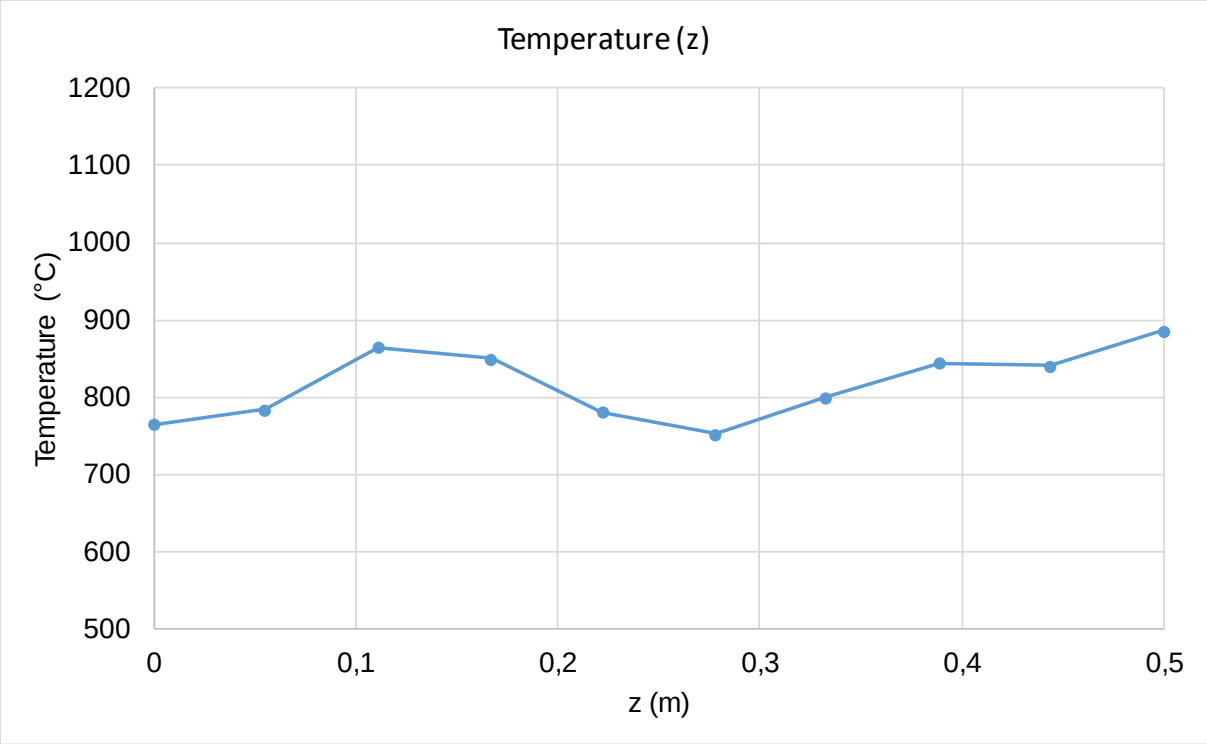

Figure 33: Peak temperatures along the rod

From Figure 34, it is shown that every peak temperature surpasses the austenization temperature. Besides, the big difference between the temperature at the center and at the side has been corrected, so now a uniform surface temperature distribution can be obtained.

Figure 35 shows the different temperature distributions for the ten simulation stages of the model, where the differences between them and their respective peak temperatures are shown.

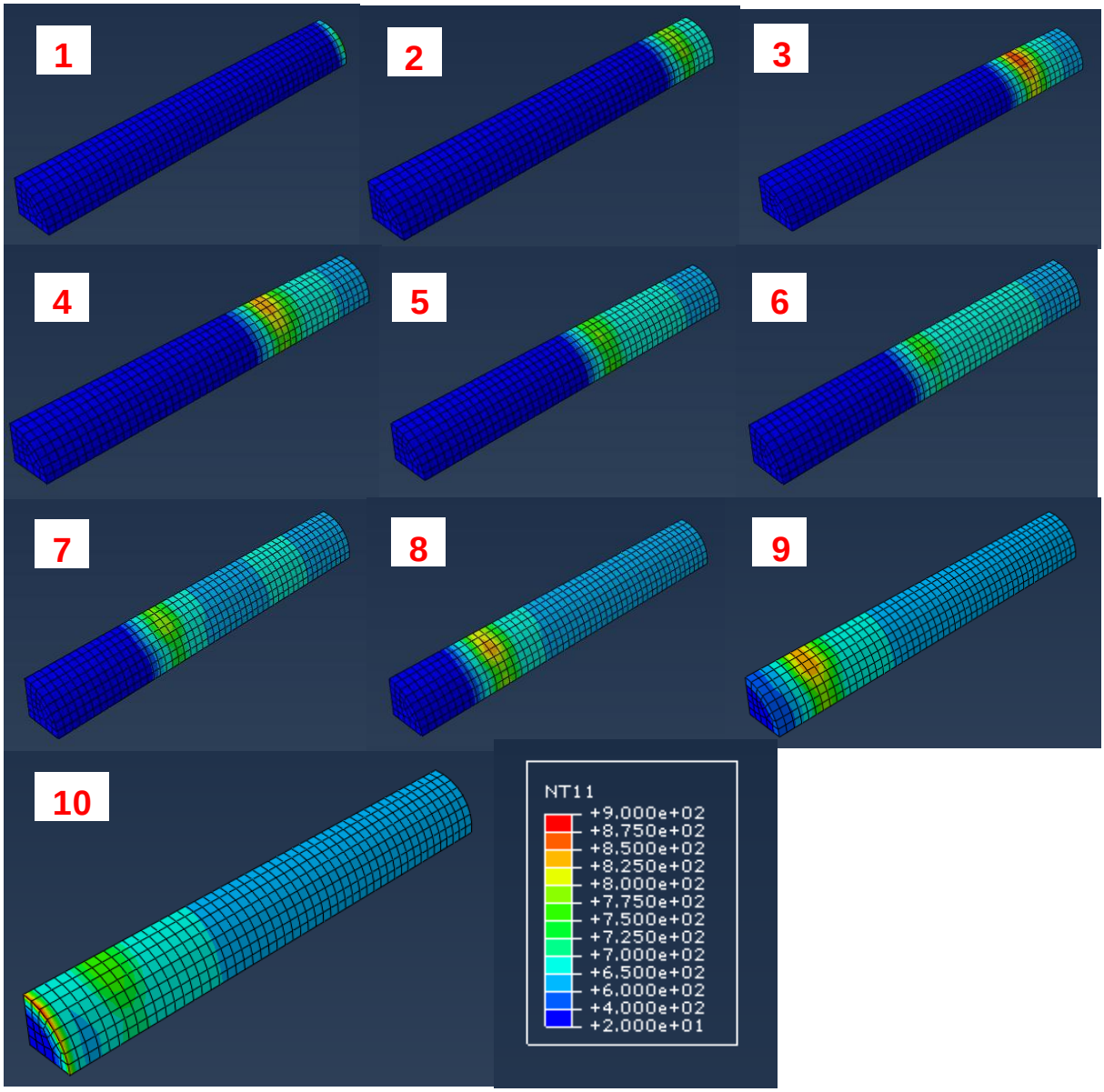

Figure 34: Temperature distributions throughout the process

Comparison between the peak temperatures of Model 3 & 4

In Figure 36 the peak temperatures along the rod from both simulations of the model are displayed.

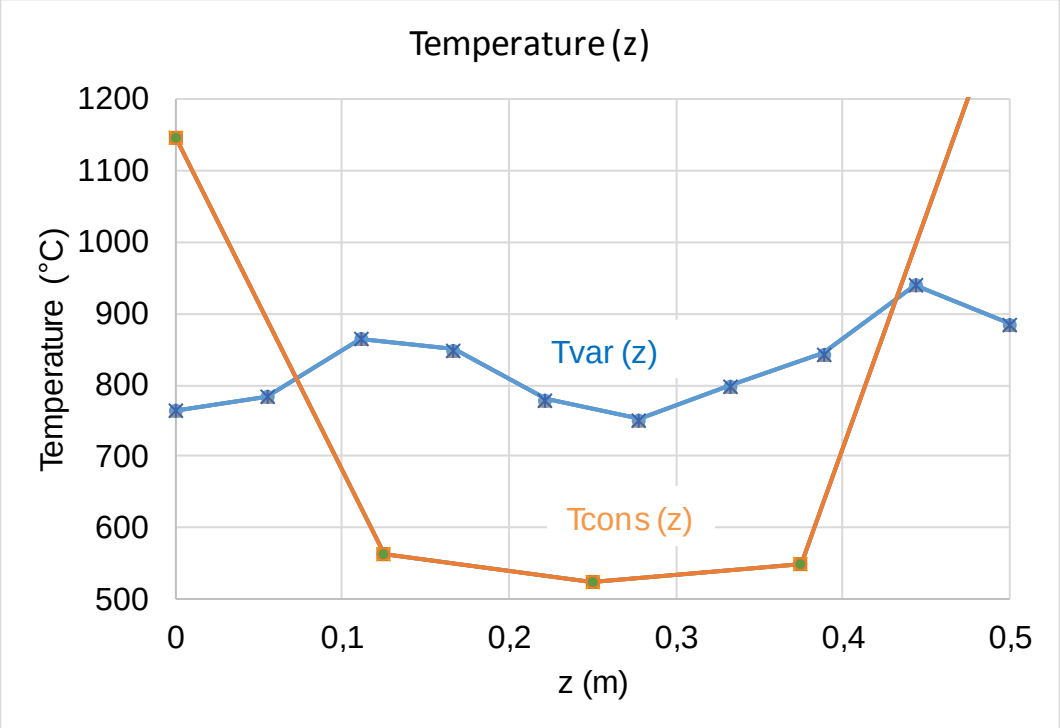

Figure 35: Comparison of temperature distributions along the rod from the moving coil model.

Figure 36 shows that this time, the temperature differences are much smaller, as the maximal peak temperature difference is 134,18°C. Also, a much lower top temperature of 886,5 °C is obtained.

Another difference from the figure is that, in the third model only the areas close to the sides surpass the austenization temperature. Therefore, with the process of the third model will be impossible to reach that temperature for the whole surface unless the process time, frequency or electric current are increased. However, this can cause overheating in the sides. Meanwhile, in the fourth model, all the temperatures are over the austenization temperature, which is another reason to use this process instead of the other one. Another ways to get the uniform temperature distribution could be using another variable process parameters apart from the velocity of the coil, like the frequency or the electric current density.

To sum up, from the comparison it can be inferred that the process with a moving coil is more suitable to harden the surface of the rod. However, the coil speed must be adjusted precisely, depending on the rod dimensions, to get a uniform temperature

distribution. To get even less dispersion of the temperature values, a more complex velocity function will be needed.

7.3 Results of the dilatometer model

The last model is a bit different from the four previous ones. As said, it consists of three simulations. The process parameters are different for the three simulations. These are shown in Table 7.

$J\ (A/m)$	$f\ (Hz)$	$t_{total}\ (s)$
$7 \cdot 10^7$	9375	34,5
$7{,}5 \cdot 10^7$	9100	17,4
$8 \cdot 10^7$	9630	7,8

Table 9: Process parameters in the dilatometer model

These electric current densities and frequencies are chosen to get the most similar temperature curve with regarding the one of the experiment.

Temperature distributions throughout the time

The simulation of the experiment is an approximation of the real heating, as the electric generator uses variable frequencies, while the harmonic simulation in Abaqus can only work with constant frequencies for the electric current. The center of the rod will be heated to 850 °C in the three cases.

In this case, the evolution of temperature is obtained for two points of the rod. These points are shown in Figure 37

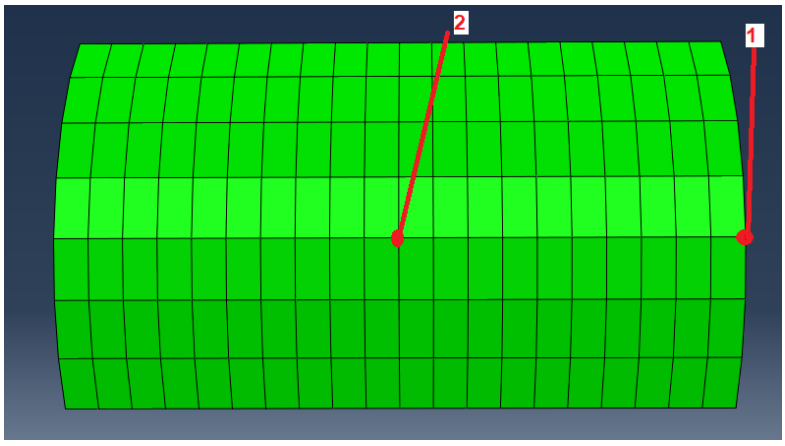

Figure 36: Points for the analysis

The evolution of temperature in both points is shown in Figure 38 for the three simulations.

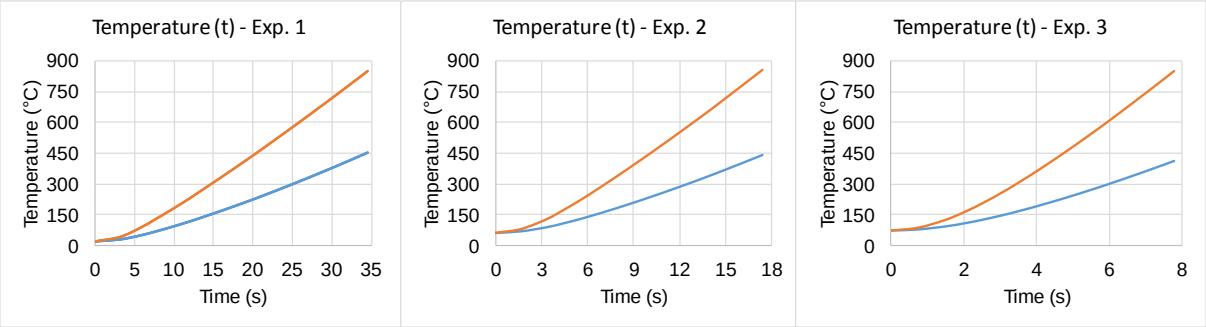

Figure 37: Temperature evolution along the time in the center (orange) and in the side (blue)

As shown, there is a big difference between the temperatures in the side and in the center. This is mainly due to the heat conduction between the rod and the subjections. The heating time has also to be taken into account. The temperature is also different between both points because the heating is very fast and, therefore, the heating time is very short. This can be seen especially in the third experiment, whose lateral temperature is lower than the temperature of the first simulation.

Differences between the model and the experiment

In the experiment, thanks to the electric generator, is possible to obtain a smaller difference between temperatures in the center and the sides. This can be done by using variable frequency, for example.

The temperature profile along the time of the simulation and of the experiment for the first heating is shown in Figure 39.

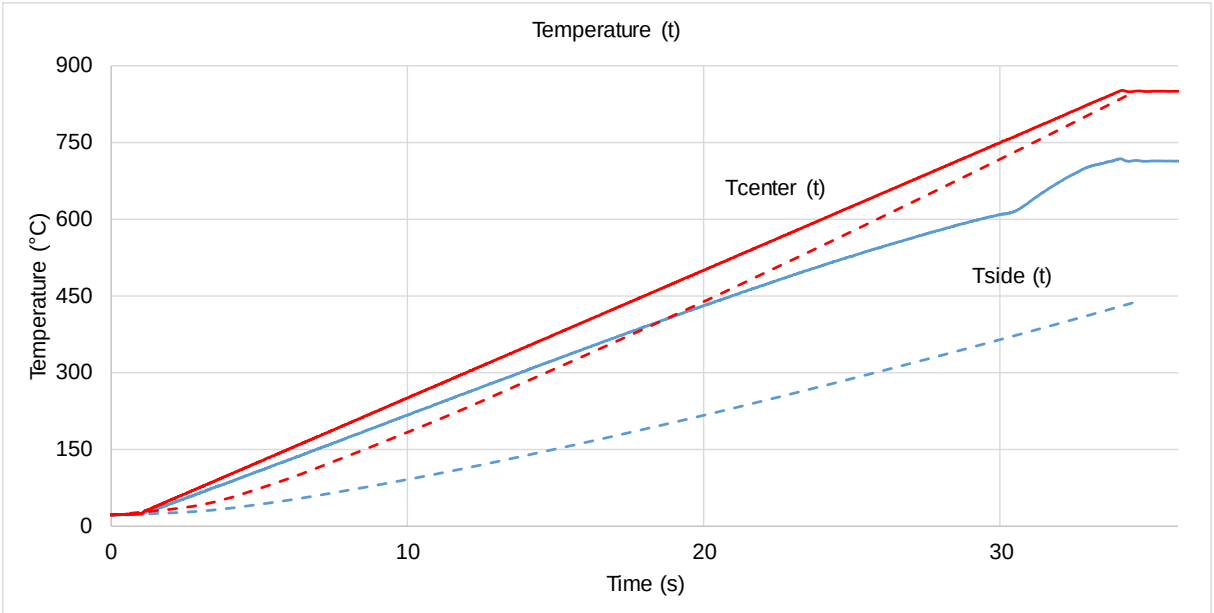

Figure 38: Temperature growth with time in the experiment (full lines) and in the simulation (striped lines)

From Figure 39 it can be seen that the heating in the center is very similar in the simulation and in the experiment. The differences between them are that the heating of the experiment has a smaller transitory, which means that the temperature is linear with time sooner than by the simulation. Also due to this, the heating rate is lower than the one of the simulation. In the side, the difference if much bigger and the final temperature is not the same.

This deviation from the simulation is due to the use of variable frequency in the experiment, because the simulation curve obtained is only the steady state response of the sample, where only a constant frequency can be used. Figure 40 shows the deviation and how the frequency changes.

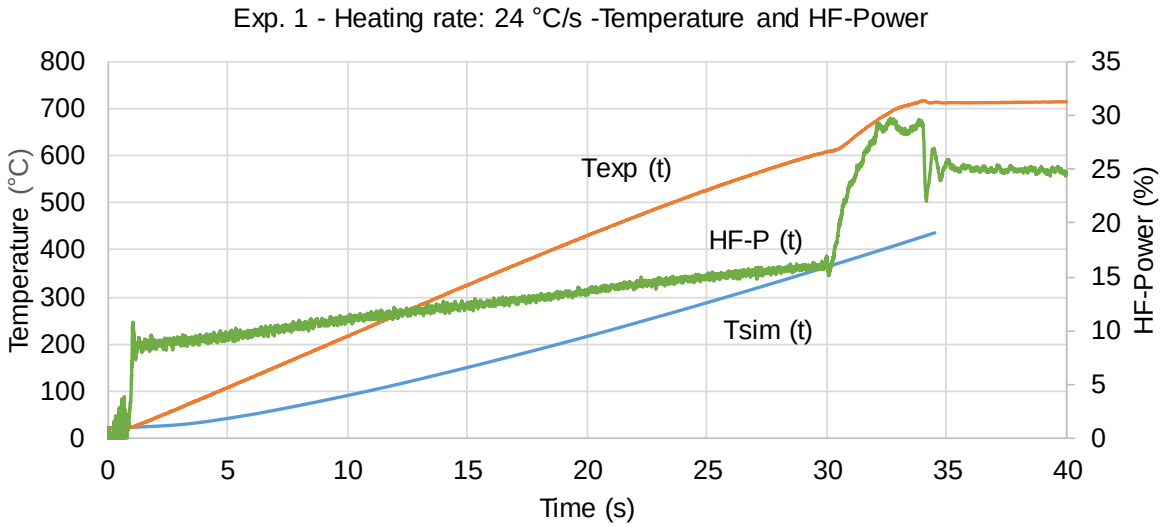

Figure 39: High frequency power and temperatures in the side with time for experiment 1

This figure shows that the frequency changes during the heating. The generator changes the frequency to adapt the power, so that the temperature variation with time can be as linear as possible. There are very big variations of the frequency especially at the beginning and at the end of the heating. The first one is done to avoid, as much as possible, the initial transient. It is shown in Figure 39. The big change at the end is done because in the experiment, after the heating, the temperature is maintained at 850ºC for some time before cooling. Figure 40 shows how this affects the temperature in the end by $t = 30\,s$, where the temperature function changes from a linear heating to a non-linear one.

The simulation temperature in the sides is different due to several reasons:

- Abaqus can only simulate the steady state curve and work with constant frequencies and powers.

- The temperature dependency of the thermal and electrical properties is not considered in the analysis, as the simulation was defined with constant values for these properties.
- The ferromagnetic behaviour of the steel is not being considered.

In the second and the third experiment happens the same, although the differences here are higher due to the faster heating. It is shown in Figure 41.

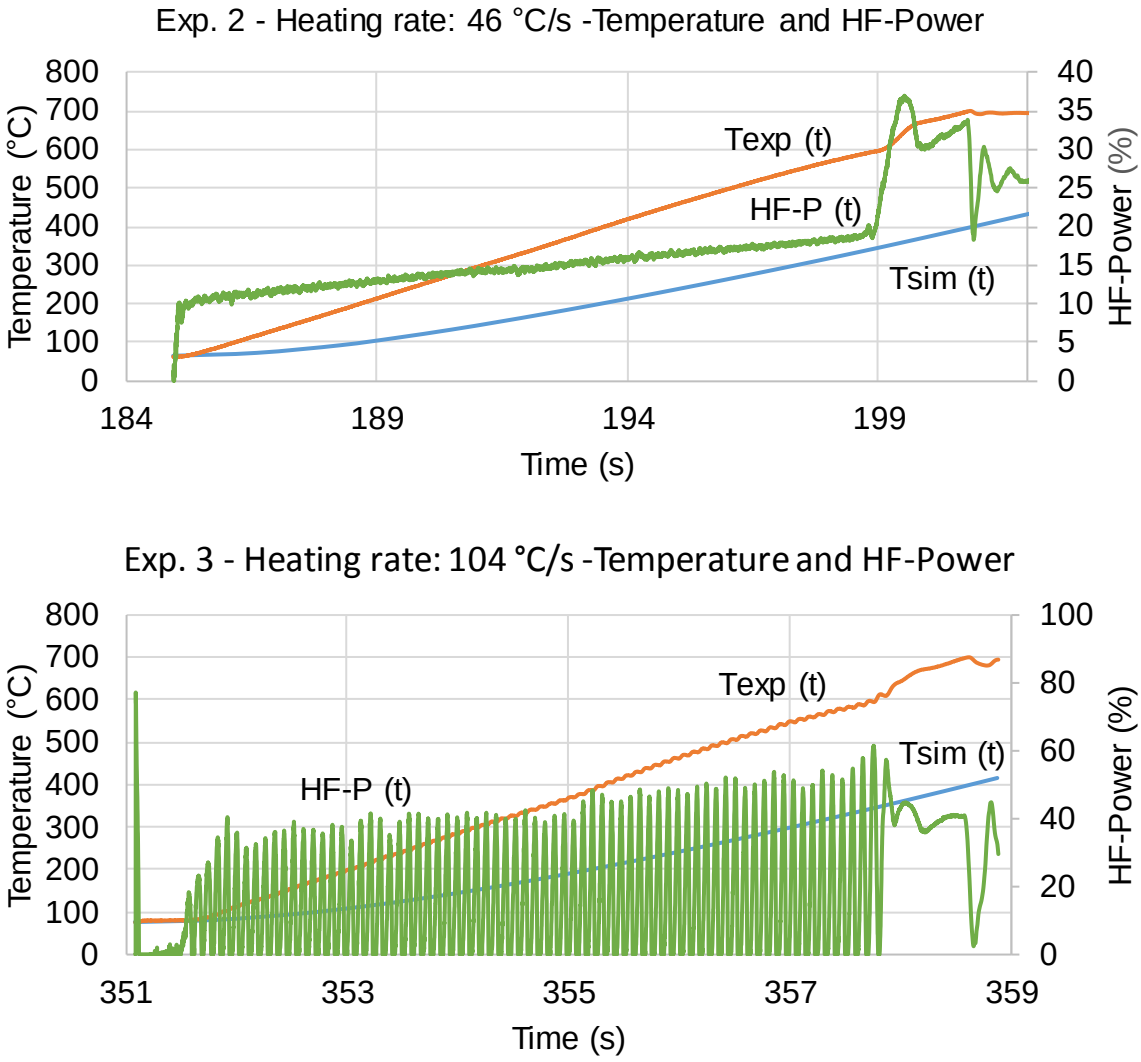

Figure 40: High frequency power and temperature in experiments 2 (up) and 3 (down)

These two figures (Figure 41) shown that the faster the heating is, the more the HF-power has to change. This can be appreciated especially in the second figure.

It is also shown that the differences between the simulation temperature (striped line) and the experiment temperature (full line) are also higher the faster the heating is. This is due to the transient response. The transient in the simulation is very similar in the three heating processes, while in the experiments is always shorter. The heating time is increasingly shorter, which means that the transient in the simulation is

increasingly longer, compared to the total heating time. The heating rate is lower during the transient, so the final simulation temperature will be lower the shorter the heating time is.

8 Conclusion

Throughout this thesis several models have been created to study the heating by induction in a steel rod. The effect of the different process parameters has been defined and verified, as well as a model has been proposed to obtain more uniform temperature distributions along the rod by adding movement to the coil. Finally, the heating of a sample in the dilatometer of the thermophysics laboratory has been simulated to check the degree of correctness of the induction heating simulations in Abaqus, as well as the difference between the temperature in the center and in the sides of the rod.

The objective of the thesis has been achieved, although some of the simulations may be insufficient to be able to apply this results to a real process. The limitations of the use of Abaqus instead of another FEM program have been seen especially in the moving coil model and the dilatometer model:

- Abaqus interactive module does not give the option of performing transient analysis without writing a script in Phython. Therefore, it was not possible to simulate a process with variable frequency.
- The movement of the coil could only be simulated by changing the step times of the sequential simulations and the position of the coil along the rod. This is also due to my own lack of knowledge in Python scripting, with which it could have been possible to simulate the movement of the coil.

However, the main objective of simulating approximately the induction heating in the rod has been fulfilled. From the results it can be inferred how to influence the temperature distribution using parameters like the frequency and the power input, as well as the coil velocity. Now, a first look at how the coil speed curve should be to obtain uniform temperature distributions was obtained. As for the last model, now it is known that Abaqus is insufficient to simulate induction heating processes with variable parameters and that is better to use another software instead, like Ansys for example.

I hope that this bachelor thesis can be used as a first approach to the simulation of induction heating processes for future thesis and investigations about this theme.

9 List of Figures

10 List of Tables

11 Bibliography

[1] RUDNEV, Valery; LOVELESS, Don; COOK, Raymond L.: Handbook of induction heating, 2nd Edition; CRC Press; 2017, Cleveland, USA.

[2] TIPLER, Paul A.; MOSCA, Gene: Física para la ciencia y la tecnología Vol. 2: Electricidad y magnetismo / Luz; Editorial Reverté, 2010, Barcelona, Spain.

[3] DAVIES, John Davies; SIMPSON, Peter: Induction heating handbook; McGraw Hill; 1979 Maidenhead, Berkshire, England

[4] ZILL, Denis G.: Matemáticas avanzadas para ingeniería, vol. 1, Ecuaciones diferenciales; 3rd Edition; McGraw Hill; 2008, Mexico D.F., Mexico.

[5] ÇENGEL, Yunus A.; GHAJAR, Afshin J.: Transferencia de calor y masa – Cuarta Edicion; McGraw Hill; 2011 Mexico D.F., Mexico

[6] AZIKI, Hicham: Masterarbeit: simulation der induktiven Erwärmung von Formplatinen; 2015, Aachen, Germany.

[7] MADRE SEDILES, Mª Antonieta; FRANCO GIMENO, José Manuel; MARTÍN SANJOSÉ, Jesús: Ingeniería de materiales para la industria y la construcción; Mira Editores; 2004, Málaga, Spain.

[8] BROECKMANN, Christoph; BEISS, Paul: Werkstoffkunde I; Rwth-Aachen University; 2018, Aachen, Germany

[9] http://www.sisa1.com.mx/pdf/Acero%20SISA%20H13.pdf, 06.08.2018

[10] http://www.steel-grades.com/Steel-Grades/Tool-Steel-Hard-Alloy/H13.html, 06.08.2018

[11] https://www.rgpballs.com/es/bolas-de-acero-al-cromo-aisi-52100-100cr6/, 06.08.2018

[12] https://matmatch.com/search?utm_source=bing&utm_medium=cpc&utm_campaign=%5BSN%5BMat_003%5D%3A%20Steel&utm_term=%2BSteel%20%2Belectrical%20%2Bproperties&utm_content=%5BMat_003%7CPro_002%5D%3A%20Electrical, 06.08.2018

[13] NIKISHKOV, G.P.: Introduction to the finite element method; University of Aizu; 2004, Aizu-Wakamatsu, Japan

[14] CALVO CALZADA; Begoña; MARTINEZ BARCA; Miguel Ángel; PEÑA BAQUEDANO, Estefanía: Apuntes de elementos finitos para solidos deformables, Universidad de Zaragoza, 2016 Zaragoza, Spain.

[15] http://www.goodfellow.com/S/Alumina.html, 06.08.2018

[16] http://abaqus.software.polimi.it/v6.14/index.html, 06.08.2018

[17] https://www.wolframalpha.com/, 06.08.2018

[18] https://www.desmos.com/calculator, 06.08.2018

[19] http://abaqus.software.polimi.it/v6.14/index.html, 06.08.2018

[20] Eser, A; Skalenübergreifende Simulation des Anlassens von Werkzeugstälen, Aachen, RWTH Aachen University, Disseration, 2014

[21] Acht, C.; Dalgic, M.; Frerichs, F.; Hunkel, M.; Irretier, A.; Lübben, Th.; Surm, H.: Ermittlung der Materialdaten zur Simulation des Durchhärtens von Komponenten aus 100Cr6 HTM, Band 63 (2008), 5, S. 234–244